Journal Pre-proofs

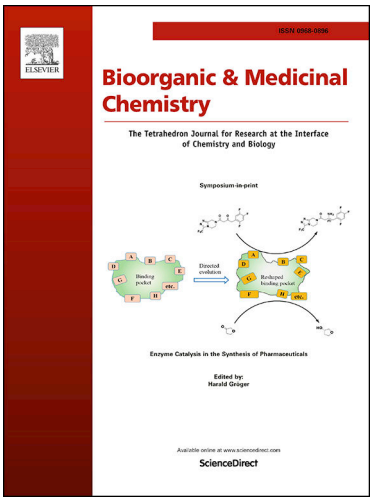

Pyrimethamine Conjugated Histone Deacetylase inhibitors: Design, Synthesis and Evidence for Triple Negative Breast Cancer Selective Cytotoxicity

Bocheng Wu, Shaghayegh Fathi, Shanee Mortley, Mahir Mohiuddin, Young C. Jang, Adegboyega Oyelere

PII: S0968-0896(20)30135-8
DOI: https://doi.org/10.1016/j.bmc.2020.115345
Reference: BMC 115345

To appear in: *Bioorganic & Medicinal Chemistry*

Received Date: 10 October 2019
Revised Date: 12 January 2020
Accepted Date: 22 January 2020

Please cite this article as: B. Wu, S. Fathi, S. Mortley, M. Mohiuddin, Y.C. Jang, A. Oyelere, Pyrimethamine Conjugated Histone Deacetylase inhibitors: Design, Synthesis and Evidence for Triple Negative Breast Cancer Selective Cytotoxicity, *Bioorganic & Medicinal Chemistry* (2020), doi: https://doi.org/10.1016/j.bmc.2020.115345

Pyrimethamine Conjugated Histone Deacetylase inhibitors: Design, Synthesis and Evidence for Triple Negative Breast Cancer Selective Cytotoxicity.

Bocheng Wu[1†], Shaghayegh Fathi[1, 2†], Shanee Mortley[1], Mahir Mohiuddin[4, 5], Young C. Jang[3, 4, 5], Adegboyega Oyelere[1, 4*]

School of Chemistry and Biochemistry, School of Biological Sciences, Parker H. Petit Institute for Bioengineering and Bioscience, Georgia Institute of Technology, Atlanta, GA 30332-0400 USA

[1]School of Chemistry and Biochemistry, Georgia Institute of Technology

[2]Current Address: University of Chicago

[3]School of Biological Sciences, Georgia Institute of Technology

[4]Parker H. Petit Institute for Bioengineering and Bioscience, Georgia Institute of Technology

[5]Wallace H. Coulter Department of Biomedical Engineering, Georgia Institute of Technology

[†]These Authors contributed equally to the manuscript

Correspondence to:

Adegboyega K. Oyelere, **E-mail:** aoyelere@gatech.edu

Keywords: Pyrimethamine, STAT proteins, STAT3, histone deacetylases, histone deacetylase inhibitors, Triple Negative Breast Cancer, molecular docking

Abstract:

Signal transducer and activator of transcription 3 (STAT3) is an oncogenic transcription factor which has been recognized as a promising cancer therapeutic target. Small molecule pyrimethamine (PYM) is a known direct inhibitor of activated STAT3 and it is currently under clinical trial. Also, histone deacetylase (HDAC) inhibition has been shown to indirectly attenuate STAT3 signaling through inhibition of STAT3 activation. Herein we described the design and biological profiling of two classes of PYM-conjugated HDAC inhibitors (HDACi). We observed that the class I PYM-HDACi compounds **12a-c** potently inhibited HDACs 1 and 6 in cell free assays while a lead class II PYM-HDACi compound **23** showed a strong HDAC 6 selective inhibition. In a cell-based assay, **12a-c** are preferentially cytotoxic to MDA-MB-231, a TNBC cell line that is highly STAT3-dependent, while **23** showed no such selective toxicity. Subsequent target validation studies revealed that a representative class I PYM-HDACi compound **12c** elicited a signature of HDAC and STAT3 pathway inhibition intracellularly. Collectively, these data suggest that PYM-HDACi compounds are promising leads to develop targeted therapy for TNBC.

Key words: Triple Negative Breast Cancer, Pyrimethamine, HDAC inhibitor, STAT3 pathway

Introduction:

Pyrimethamine (PYM) (Figure 1) is an FDA approved drug which, due to its perturbation of the functions of several intracellular targets, has found use for the management of various human diseases including toxoplasmosis and malaria.[1,2] PYM has also been used in chemotherapy along with other drugs such as proguanil for few decades.[3] PYM's anti-parasitic activity originates from its ability to specifically bind and inhibit dihydrofolate reductase (DHFR, 5,6,7,8-tetrahydrofolate: $NADP^+$ oxidoreductase, EC 1.5.1.3) in *Plasmodium falciparum* and other protozoa.[4] DHFR is critical for folate metabolism and has been a drug target for fungal, protozoal and bacterial infections and cancer. DHFR facilitates an NADPH-dependent reduction of dihydrofolate to tetrahydrofolate, a cofactor necessary for the biosynthesis of thymidylate, purine nucleotides, and many other essential amino acids required for protein, RNA, and DNA synthesis.[5] DHFR inhibition by antifolate compounds interferes with these pathways, resulting in cell cycle arrest and cell death.[6]

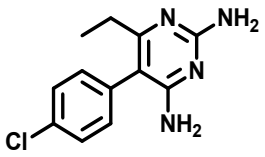

Figure 1. Structure of pyrimethamine.

PYM is also an inhibitor of STAT3 (Signal transducer and activator of transcription 3) transcriptional function.[7] STAT3 is a member of STAT proteins comprising of seven sub-family members (STAT1, 2, 3, 4, 5a, 5b, 6).[8] STAT3, an oncogenic transcription factor with critical role in the signaling of a number of cytokines and growth factors, confers resistance to apoptosis in various cell types[9] and is activated in many cancers including triple-negative breast cancer

(TNBC), acute myeloid leukemia (AML), chronic lymphocytic leukemia (CLL) and small lymphocytic lymphoma (SLL).[10,11]

STAT3 activation through its tyrosine phosphorylation by JAK (Janus kinase) or IL-6 signaling cascade[12] enhances its dimerization and translocation from cytoplasm to nucleus where it can bind to certain DNA sequences and regulate genes expression involved in various cellular processes. Tyrosine phosphorylation is not the only way to activate STAT3. It can be activated through other processes such as serine phosphorylation, acetylation, methylation, and glutathionylation.[13,14] Once STAT3 is activated, it enhances various cell processes such as cell proliferation, differentiation, survival, and angiogenesis that contribute to malignant transformation and progression in many cancers such as breast, ovary, and prostate.[15] Although STAT3 also has non-transcriptional responsibilities, such as regulation of mitochondrial function, most of its oncogenic activities are related to its gene regulation in the nucleus.[16]

Activation of STAT3 is tightly regulated in normal conditions; however, in cancer, it is highly activated and leads to malignant cancer cells phenotype.[17] Therefore, inhibiting STAT3 activation is a promising strategy for cancer therapy, as several cancer types depend on activated STAT3 for their survival. In fact, PYM is currently in phase I/II clinical trials as a standalone agent for the treatment of relapsed CLL and SLL (ClinicalTrials.gov Identifier: NCT01066663). Interestingly, however, it has been observed that STAT3 inhibitors exhibit a synergistic effect with other therapeutic agents in inhibiting tumor stem cells, leading to improved therapeutic indices for these agents.[18]

Histone deacetylase (HDAC) enzymes are a class of proteins that play an important role in regulating STAT3 activation.[19] HDACs, along with histone acetyltransferase (HAT), control gene expression, chromatin condensation and play an essential role in transcriptional activation by

regulating acetylation state of histone proteins.[20] In addition to histones, the expression levels and acetylation status of several non-histone proteins, including transcription factors (E2F, STAT3, P53, NF-κB), estrogen receptor (ERα), androgen receptor (AR), α-tubulin, and chaperons (HSP90), are regulated by HDAC and HAT activity.[21] Due to their critical roles in regulating a wide range of cellular pathways, HDACs are considered as promising drug discovery targets, and their inhibition has emerged as a potential strategy in treating various diseases including neurological diseases, malaria, leishmania and cancer.[22] To date, there are four US FDA approved HDAC inhibitors (HDACi), namely, SAHA (suberoylanilide hydroxamic acid, vorinostat) approved in 2006 for relapsed and refractory cutaneous T-cell lymphoma (CTCL),[23] romidepsin (FK228) approved in 2009 for relapsed/refractory peripheral T-cell lymphoma,[24] belinostat (PXD101) approved in 2014 for relapsed/refractory peripheral T-cell lymphoma,[25] and panobinostat (LBH589) approved in 2015 for treating acute myeloma (Figure 2).[26] Chidamide (CS055) is another HDACi which is approved in China for treating relapsed/ refractory peripheral T-cell lymphoma. Chidamide is in phase II clinical trials in the US.[27] Inhibition and knockdown of class I HDACs have been shown to result in inhibition of STAT3 activation, through upregulation STAT3 Lys685 acetylation and attenuation of STAT3 Tyr705 phosphorylation, resulting in the inhibition of the survival of pSTAT3-positive lymphoma (DLBCL) cells.[28] Therefore, targeting STAT3-positive cancer cells with HDACi is another potentially viable therapeutic option for managing these tumors. Inhibition of STAT3 pathway has been mediated by HDACi SAHA through the acetylation on bromodomain protein 4 (BRD4) to down-regulate Leukemia Inhibitory Factor Receptor (LIFR).[29]

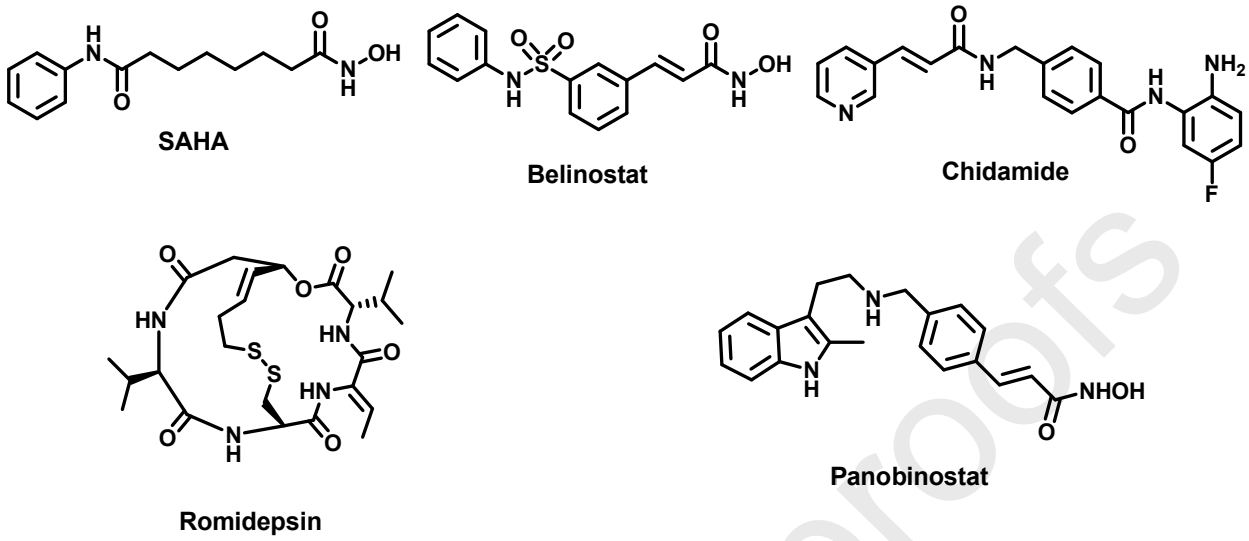

Figure 2. Structures of approved HDACi.

We hypothesized that designed multiple ligands comprising PYM and HDAC inhibition chemotype would integrate direct STAT3- and HDAC-inhibition within a single molecular template. These PYM-HDACi compounds are anticipated to be efficient inhibitors of proliferation of tumors which are exquisitely dependent on STAT3 signaling pathway. Herein we demonstrate that PYM-HDACi compounds inhibit representative HDACs, downregulate the expression of selected STAT3 target proteins and are selectively cytotoxic to MDA-MB-231, a triple-negative breast cancer (TNBC) cell that is highly dependent on STAT3 Pathway for its proliferation and metastasis.

Results and discussion

Design of PYM-HDACi compounds

The three-motif HDACi pharmacophoric model consists of a recognition cap group, linker group, and zinc-binding group (ZBG) (Figure 3).[30] PYM structure closely resembles the HDACi aryl-derived cap group. Our molecular docking analysis (discussed below) suggested that the PYM halogen group could be replaced by the HDACi linker and ZBG groups without significantly impacting STAT3 binding. Interestingly, the substitution of the PYM halogen group with alkyl, aryl, and ring systems have been shown to be compatible with its biological activities.[31] Based on these observations, we designed two classes of PYM-HDACi compounds using PYM as a surrogate for HDACi cap group. The restriction on the length of the linker group of class I compounds is based on our previous study which revealed that five and six methylenes are an ideal length for linker group for aryl triazolyl HDACi which inspired the design of this class of compounds.[22] Relatedly, the linker group of class II compounds is based on a similar moiety in the approved HDACi belinostat and panobinostat.

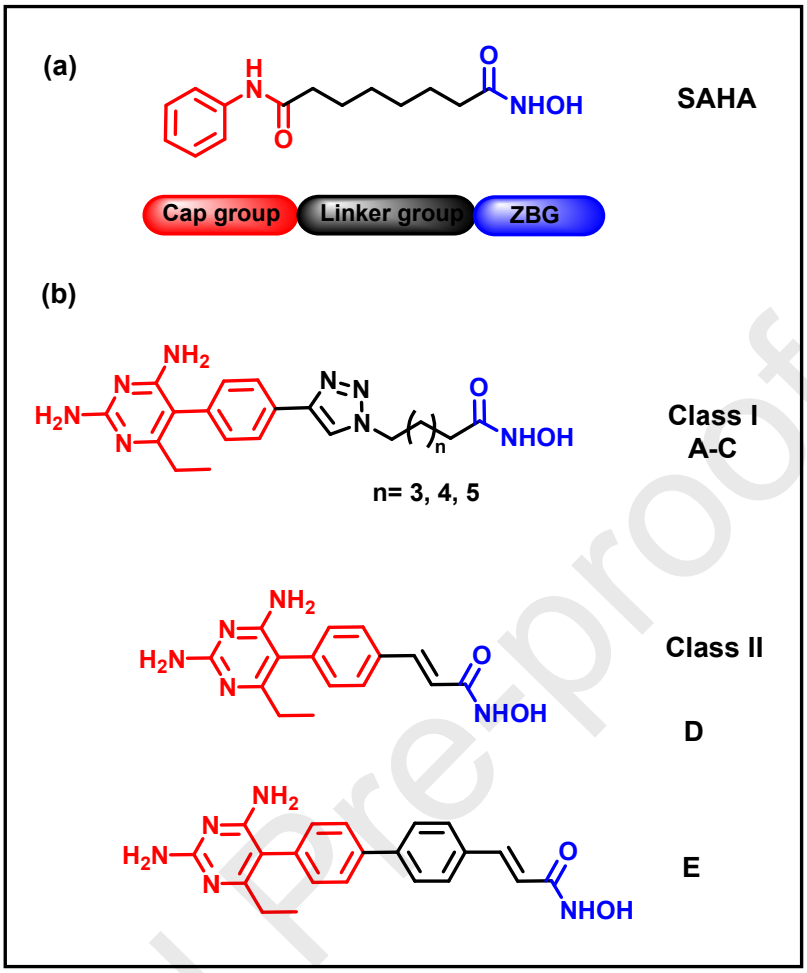

Figure 3. (a) Pharmacophoric model of HDACi using SAHA as a prototypical HDACi. (b) Structures of the designed two classes of PYM-HDACi compounds.

Molecular docking study

We first performed an unbiased molecular docking, using AutoDock Vina,[32] to determine the potential docking poses of PYM on the structure of STAT3 (PDB ID: 1BG1). The docking outputs revealed that PYM binds to two pockets (P1 and P2) within the DNA binding domain (DBD) and one solvent-exposed, shallow pocket (P3) between the connector (a part of DBD) and the SH2 domains of STAT3 (Figure 4). Although PYM is accommodated through stabilizing H-

bonding and hydrophobic interactions with key residues within P1, P2 and P3, the binding energies of PYM at the three sites revealed a strong preference for P2. In P1 and P2, the halogen moiety of PYM is oriented in regions adjoining solvent-accessible grooves/sub-pockets which could potentially accommodate the substitution of the halogen by the HDACi linker and ZBG groups of the designed PYM-HDACi compounds (Figure 3). Conversely, in P3, the halogen moiety of PYM is tucked into a shallow pocket, an orientation which may necessitate an extensive change in the binding orientation for the PYM-HDACi to be accommodated at this location. Subsequent docking of a representative class I PYM-HDACi compound **B** revealed that it adopts similar docking poses as PYM at P1 and P2. At P3, however, the phenylpyrimidinediamine end of **B** is forced out into the protein surface to accommodate its HDAC inhibition moiety. Interestingly, **B** binds to P1 and P2 with enhanced binding affinities relative to PYM (Figure 4). This observation strongly suggests that the replacement of the PYM halogen group by the designed HDAC inhibiting moieties is compatible with the STAT3 binding attributes of PYM at P1 and P2.

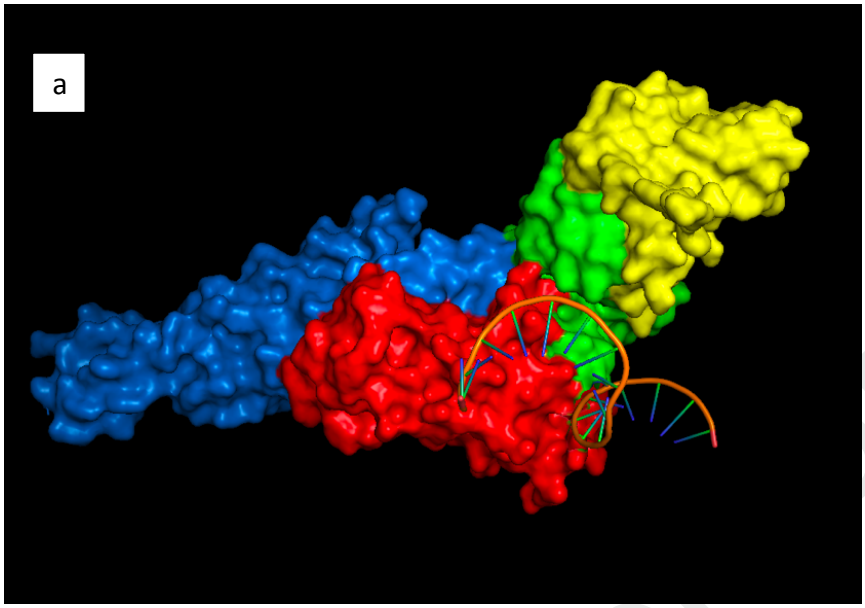
a

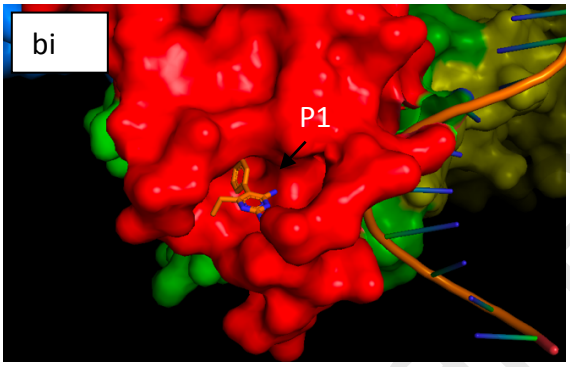
bi
P1

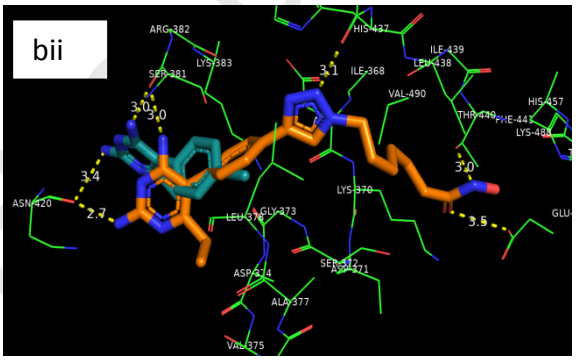
bii
ARG-382
HIS-427
ILE-439
LYS-383
LEU-438
SER-381
ILE-368
VAL-490
HIS-457
THR-440
PHE-441
LYS-483
ASN-420
LYS-370
GLY-373
LEU-376
ASP-374
ALA-377
VAL-375

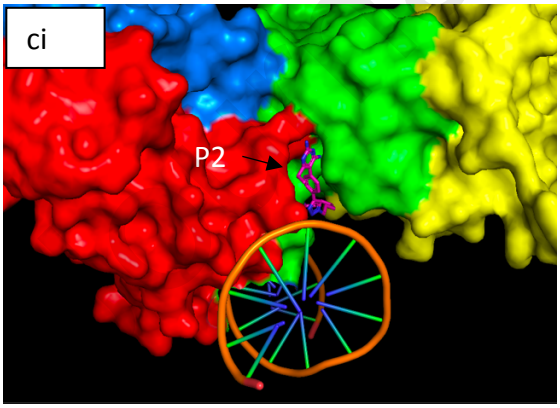
ci
P2

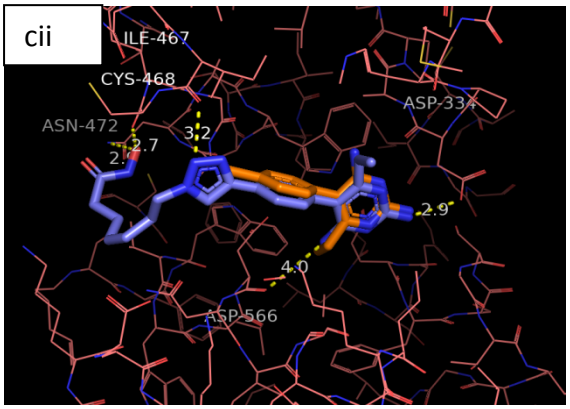
cii
ILE-467
CYS-468
ASP-334
ASN-472
3.2
2.9
4.0
ASP-566

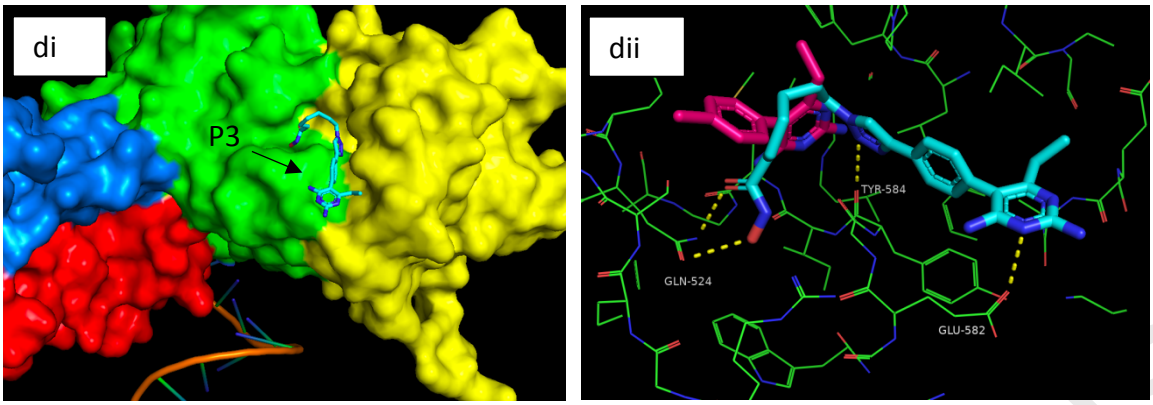

Figure 4. Molecular docking of PYM and class I PYM-HDACi compound **B** to STAT3 (PDB:1BG1). (a) The 4 domains of the STAT3 – 4-Helix bundle (blue), β–barrel (red), connector (green) and SH2 (yellow) domains. Docked poses of PYM and class I compound **B** at P1 (bi-ii), P2 (ci-ii) and P3 (di-ii). The binding energies of PYM at P1, P2 and P3 are -5.6kcal/mol, -6.4kcal/mol and -6.0kcal/mol respectively, while B bound to P1, P2 and P3 with binding energies of -9.2kcal/mol, -9.3kcal/mol and -7.3kcal/mol, respectively. Note that the binding of compound **B** to P1 could be potentially stabilized by H-bonding interactions with Ser-381, Asn-420, His-437, Thr-440, and Glu-455. In P2, compound **B** could form stabilizing H-bonding interactions with Asp-334, Ile-467, Cys-468, Asn-472 and Asp-566. In P3, compound **B** could form H-bonding interactions with Gln-524, Glu-582 and Tyr-584.

To confirm that the PYM could act as a surrogate for HDACi cap group, we performed molecular docking analyses to interrogate the interaction between the designed PYM-HDACi and selected HDAC isoforms. We observed that, in addition to engaging in stabilizing H-bonding interaction with enzymes' outer rim residues, class I compounds **B** and **C** adopt poses that may allow effective chelation of zinc ion in the active sites of HDAC 1 and HDAC 6 (Figures 5 and 6). In both HDAC 1 and HDAC 6, class I compound **B** shows strong evidence of zinc ion chelation in the pocket. Presumably due to its flexible linker, class I compound **B** is able to facilely access

the pockets of both enzymes, allowing efficient chelation of the active site zinc ion which is a key driver of HDAC 1 binding by both classes of compounds. Relative to Class II compounds **D** and **E**, the hydroxamate group of **B** seems to be positioned to allow a more efficient zinc ion chelation at HDAC 1 active site. The somewhat less optimal zinc ion chelation by **D** and **E** could be partially compensated by the possibility of formation of π–π interaction with rings of Phe-155 and Phe-210 (Figure 5). Nevertheless, the rigidity of **D** and **E** constrained their phenylpyrimidinediamine moiety to be presented on HDAC 1 surface where there is no obvious prospect for stabilizing interactions. In contrast, the flexibility of the alkyl linker of **B** allows its phenylpyrimidinediamine moiety to be tucked into a hydrophobic patch on HDAC 1 surface where it is further stabilized by a hydrogen bonding interaction with Glu-203. This *in silico* observation suggests that compound **B** could be better accommodated at HDAC 1 active site than **D** and **E**. Interestingly, the extra benzene ring of class II compound **E** is able to overcome the deficiency of class II compound **D** as it enables better zinc ion chelation and optimal binding within hydrophobic regions at outer rims guarding the active sites of HDAC 6. Specifically, compound **E** could potentially form two π–π interactions with Phe-202 and Trp-261 while compound **D** docked poses could only support one π–π interaction with Phe-202. Also, compound **B** could form H-bonding with the amide backbone of Ser-259 at the enzyme rim. The extra interactions displayed by **B** and **E** could confer on them better binding affinities for HDAC 6 relative to compound **D**.

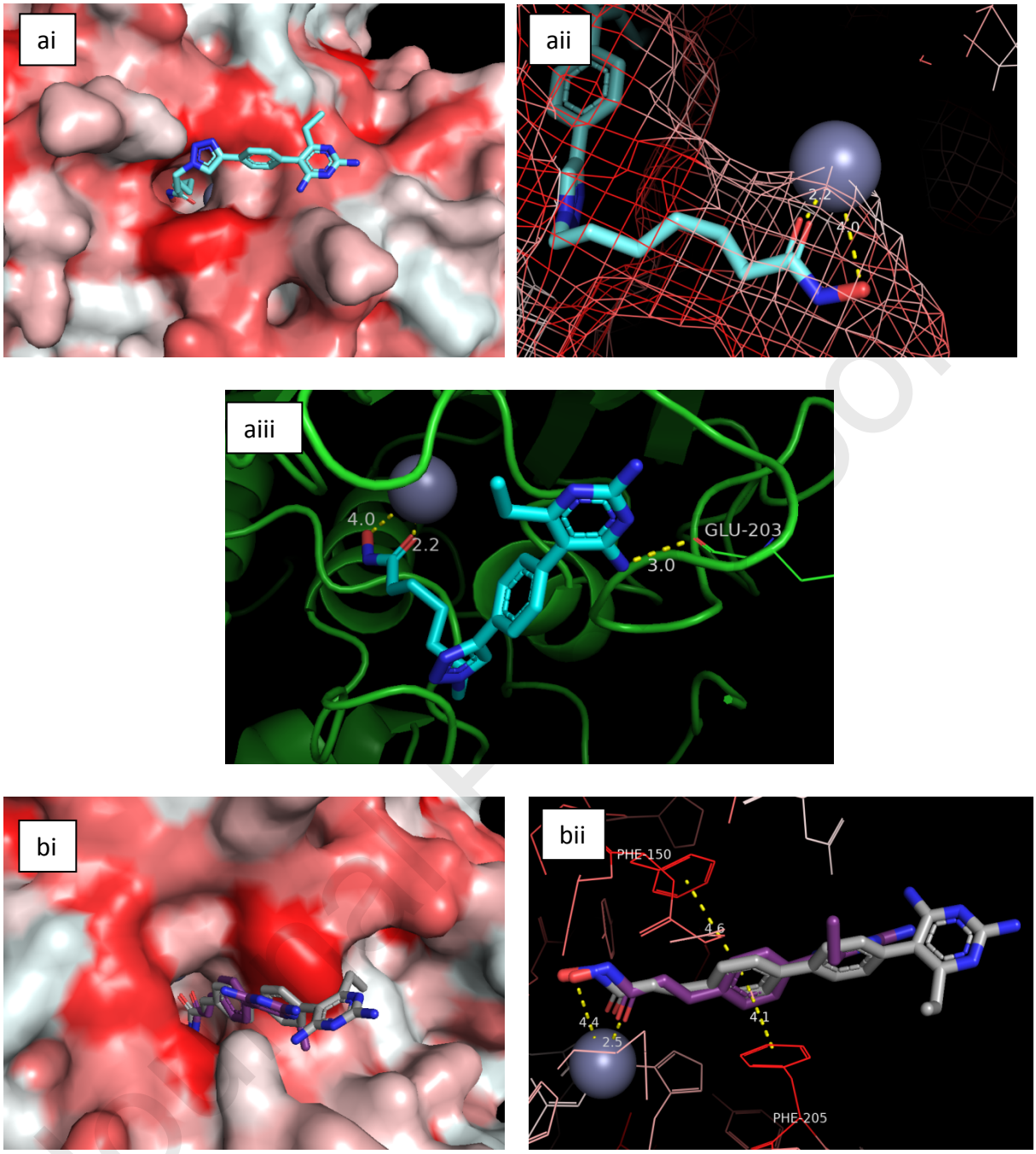

*Note that the red portion of the protein surface indicates hydrophobic and white area indicates the hydrophilic areas.

Figure 5. Docked poses of PYM-HDACi at the active sites of HDAC 1 (PDB:5ICN). Grey sphere represents zinc ion in the active site of HDAC isoform. (ai-iii) Docked pose of class I compound **B** on HDAC 1. (bi-ii) Overlay of the docked poses of class II compounds **D** (in purple) and **E** (in

grey) on HDAC 1. The compounds are accommodated at enzyme's active site through a combination of zinc chelation, H-bonding and hydrophobic interactions.

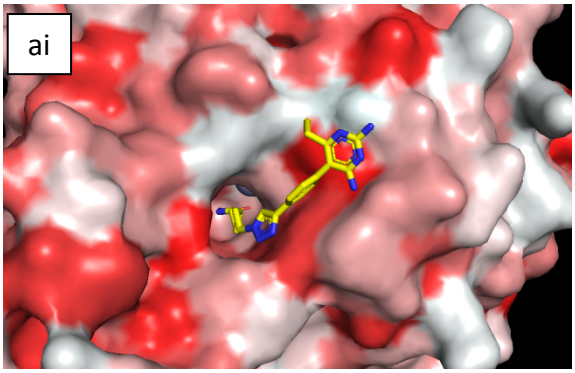

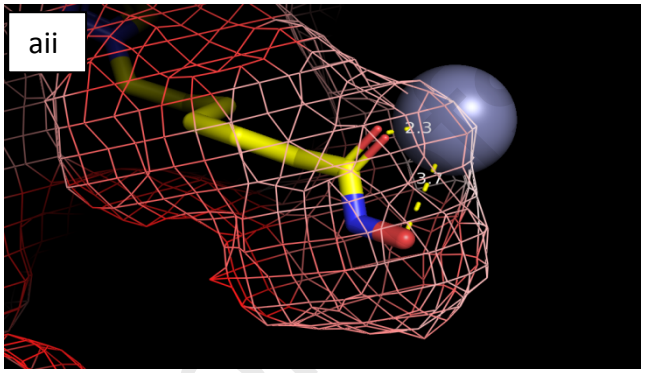

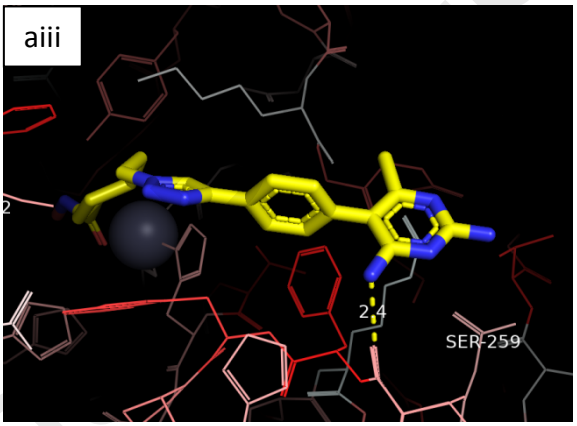

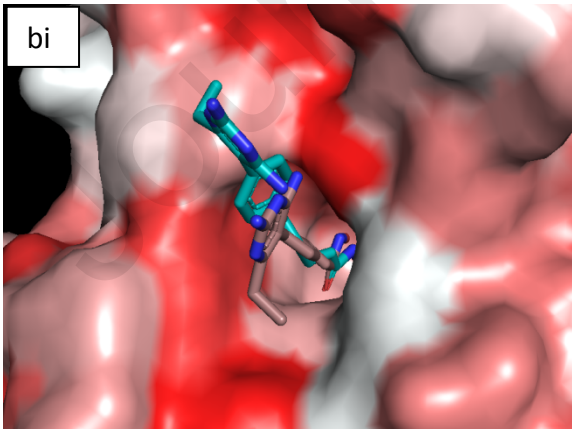

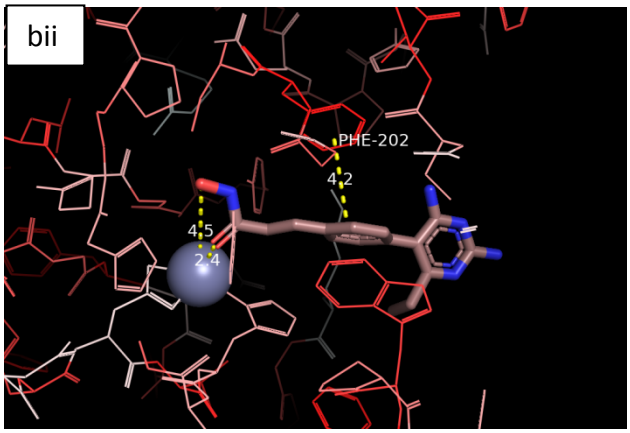

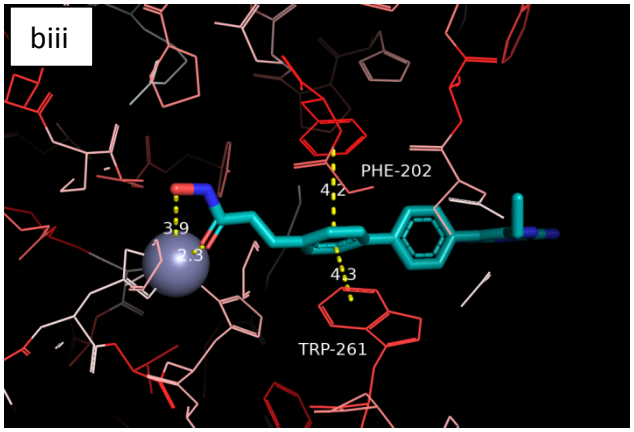

Figure 6. Docked poses of PYM-HDACi at the active sites of HDAC 6 (PDB:5G0G). Grey sphere represents zinc ion in the active site of HDAC isoform. (ai-iii) Docked pose of class I compound **B** on HDAC 6. (bi-iii) Overlay of the docked poses of class II compounds **A (**color in light pink) and **B** (color in cyan) on HDAC 6. The compounds are accommodated at enzyme's active site through a combination of zinc chelation, H-bonding and hydrophobic interactions. *Dotted lines indicate interatomic distance for H-bonding and stacking interaction.

Based on evidence from the previous molecular docking analysis on human DHFR (hDHFR),[33] it seemed that the replacement of the halogen group of PYM may not be compatible with DHFR binding. Nevertheless, we docked these compounds against the structure of hDHFR (PDB code 1U72). We observed that the PYM moiety of the PYM-HDACi compounds bind hDHFR with similar orientation as PYM (Figure S1). However, the PYM-HDACi compounds' pyrimidinediamine head does not gain access into the hDHFR binding pocket as efficiently as PYM, largely due to the interruption caused by their HDACi moiety. This result suggests that the docked poses of PYM-HDACi may not be favorable thus making DHFR inhibition a less likely attribute of the PYM-HDACi compounds.

Chemistry

To synthesize the class I PYM-HDACi compounds, 4-bromophenyl acetonitrile **1** was reacted with ethyl propanoate **2** under basic condition to yield β-ketonitrile[34] **3** which was then converted to the methoxyphenol **5** using trimethyl orthoformate **4**.[35] Pyrimidine ring was formed through cyclization reaction of **5** with guanidine hydrochloride to afford compound **6.**[31] Boc protection of amine[36,37] groups of **6**, to give **7**, followed by sonogashira reaction with trimethylsilylacetylene **8** resulted in compound **9**.[38] Trimethylsilyl group was removed using potassium carbonate to afford alkyne **10**. Subsequently, copper (I) catalyzed azide-alkyne-cycloaddition (AAC)[39] reaction between alkyne **10** and compounds **11a-c**,[40] followed by removal of trityl- protecting group resulted in the final class I compounds **12a-c**. Control compound **12d** was similarly synthesized from Boc deprotected compound **10a** and azido ester **11d** (Scheme 1).

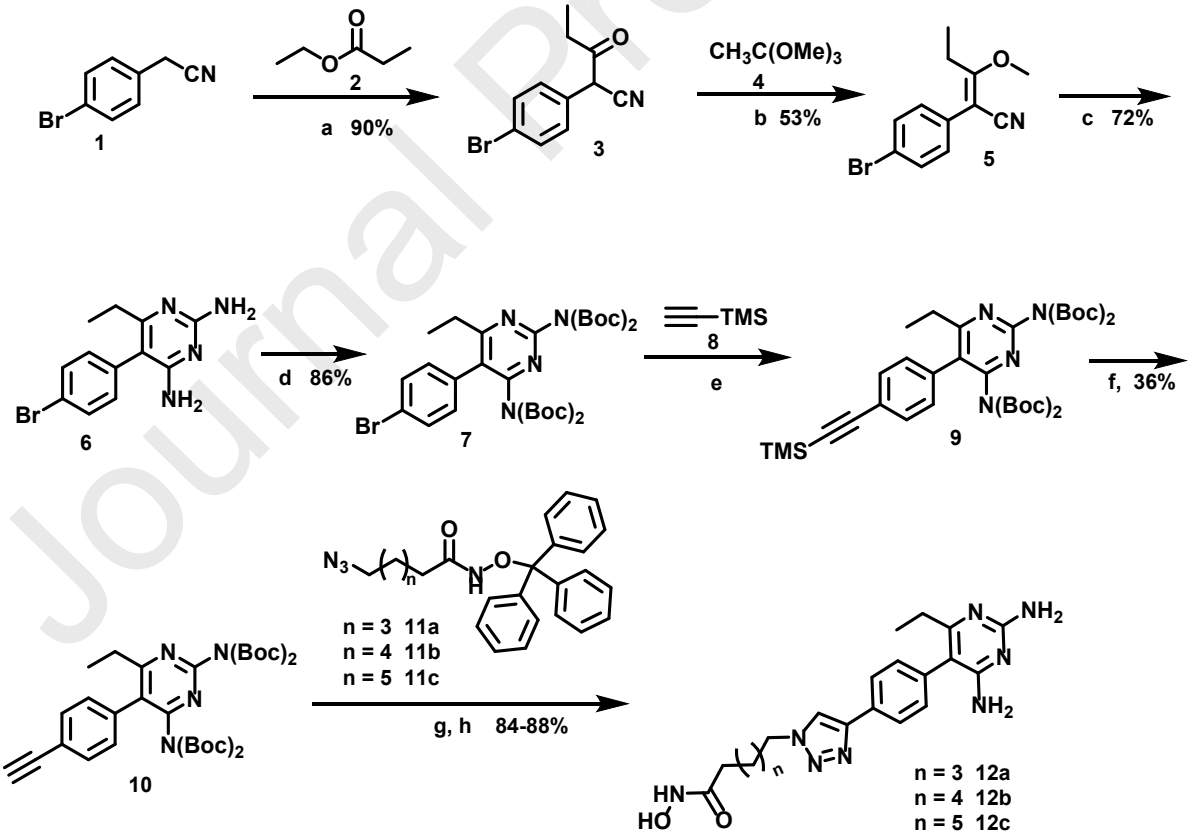

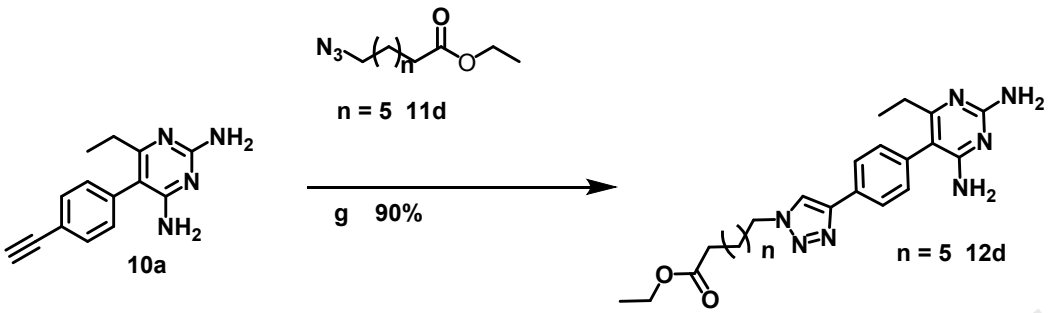

Scheme 1. (a) Potassium tert-pentylate 25% in toluene,THF, rt, 20 min, 90%; (b) 6 h, neat reaction 120 °C, 53%; (c) Guanidine hydrochloride, $NaHCO_3$, DMSO, 100 °C, 6 h, 72%; (d) Boc_2O, THF, DMAP, 45 °C, THF, 86%; (e) Hunig's base, $Pd(PPh_3)_4$, acetonitrile, CuI, 75 °C, overnight; (f) K_2CO_3, MeOH, 0 °C, 2 h, 36% (e and f); (g) CuI, Hunig's base, rt, overnight; (h) TFA, DCM, rt, 2 h, 84-88% (g and h).

To synthesize the monophenyl class II PYM-HDACi compound, a Heck reaction was performed on intermediate **6** with methyl acrylate **13**.[41] After the Boc protection to give intermediate ester **15** which was subsequently converted to carboxylic acid **16** using sodium hydroxide.[42] The desired hydroxamic acid compound **18** was synthesized through the coupling of carboxylic acid **16** and *O*-trityl hydroxylamine **17** followed by trityl deprotection (Scheme 2).[40]

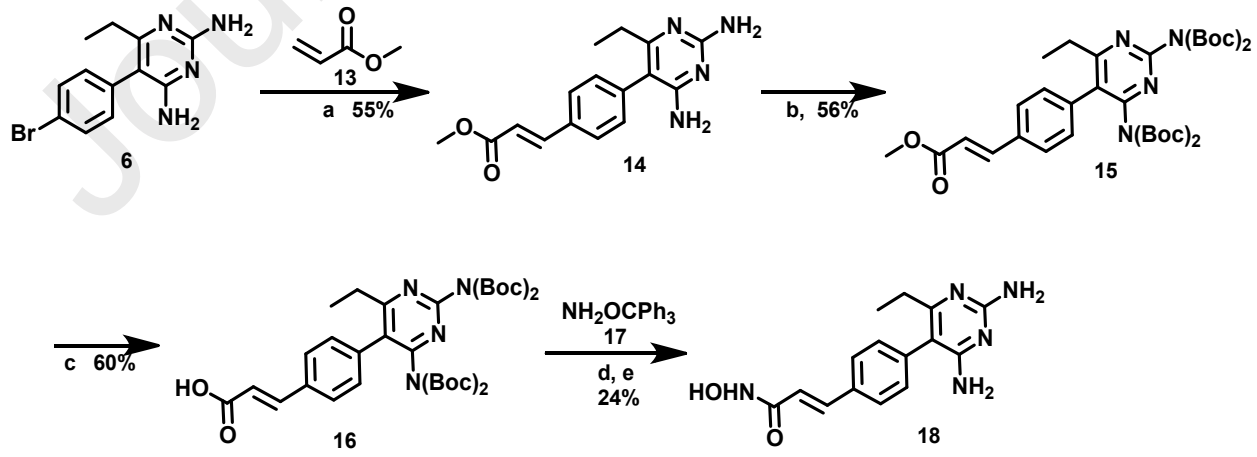

Scheme 2 . (a) Tri-*O*-tolyl phosphine, $Pd(OAc)_2$, TEA, DMF, 120 °C, overnight, 55%; (b) Boc_2O, THF, DMAP, 45 °C, THF, 56%; (c) NaOH, H_2O, Dioxane, 20 °C, 12 h, 60%; (d) EDCI, HOBT, DCM, rt, 6 h; (e) TFA, DCM, rt, 2 h, 24% (d and e).

To synthesize the biphenyl class II PYM-HDACi compound, a Suzuki coupling reaction of Boc protected intermediate **7** with 4-hydroxyphenyl boronic acid furnished compound **19** which was converted to triflate compound **20** using standard protocol. Suzuki coupling between compound **20** and potassium vinyl trifluoroborate furnished aryl vinyl compound **21**. Cross metathesis reaction of **21** with N-(trityloxy)acrylamide using Hoveyda-Grubbs 2nd generation catalyst[43] afforded compound **22** which upon treatment with TFA and TIPS furnished the desired class II compound **23** (Scheme 3).

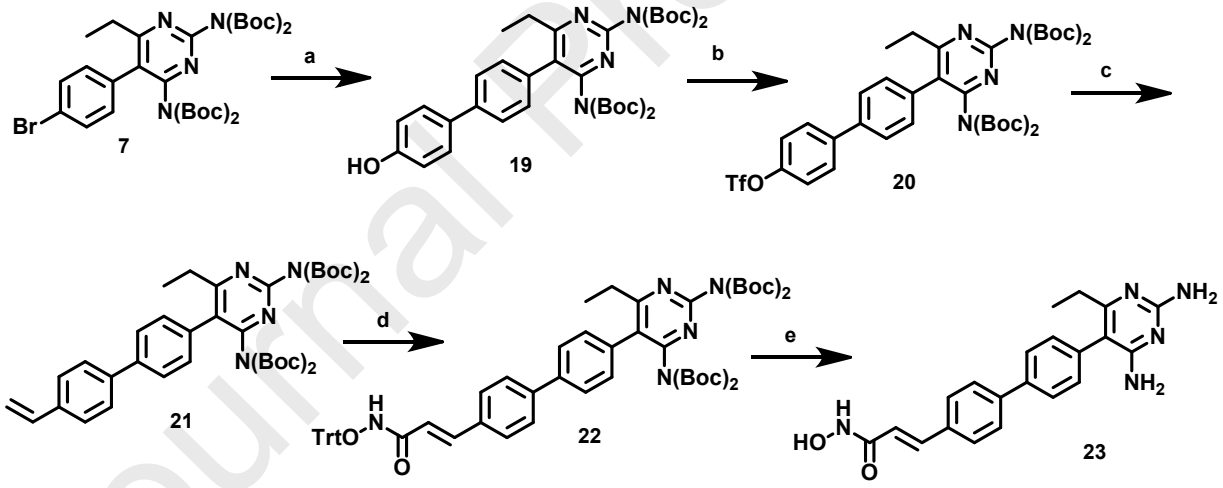

Scheme 3. (a) 4-hydroxyphenyl boronic acid, $Pd(PPh_3)_4$, Cs_2CO_3, 80 °C, 4 h, 81%; (b) Trifluoromethanesulfonic anhydride, pyridine, -20 °C, 1 h, 77%; (c) $Pd(PPh_3)_4$, Potassium vinyl trifluoroborate, Cs_2CO_3, DMF, 80 °C, 4 h, 90%; (d) Hoveyda-Grubbs 2nd generation catalyst, N-[Tris(hydroxymethyl)-methyl]acrylamide, DCM, 33°C, overnight, 33%; (e) TFA, TIPS, rt, 2 h, 80%.

HDAC inhibition study

PYM-HDACi compounds were tested against HDAC isoforms 1, 6 and 8. These compounds inhibited the HDAC isoforms tested with IC_{50}s ranging from low nanomolar to micromolar. Specifically, class I compounds **12a-c** broadly inhibited HDACs 1 and 6 but are less potent against HDAC 8 (Table 1). Within this class, there is a linker length dependency in HDAC 1 and 6 inhibition potency which optimal for compound **12b**. The monophenyl class II compound **18** is a relatively weaker HDACi which displayed the strongest inhibitory effect towards HDAC 6. The inclusion of an additional phenyl ring, however, broadened and enhanced potency as the biphenyl class II compound **23** inhibited both HDAC 6 (Table 1). This HDAC inhibition pattern is in agreement with the predictions from the in silico docking study shown in Figures 5 and 6.

Table 1: HDAC inhibition activities of PYM-HDACi compounds (IC_{50} in μM).[a]

Compound	HDAC1	HDAC6	HDAC8
12a	0.26	0.046	2.8
12b	0.045	0.017	0.78
12c	0.21	0.021	NT[b]
18	2.2	0.40	1.8
23	3.7	0.073	NT
SAHA	0.042	0.034	2.8

[a]Performed through contractual agreement with BPS Bioscience. [b]NT: Not Tested.

Anti-proliferative activity

The PYM-HDACi compounds were tested against three transformed and one normal cell lines with SAHA, an FDA approved HDACi, as a positive control. The chosen transformed cell lines were lung (A549), ER-positive (MCF-7) and TNBC (MDA-MB-231) breast cancer cell lines, while monkey kidney epithelial cell (VERO) was selected as the nontransformed cell line. Our choice of the transformed cell lines is informed by the STAT3 pathway dependency of these cell lines. TNBCs, which account for 20% of all breast cancer incidence, lack Estrogen Receptor (ER), Human Epidermal Growth Factor receptor 2 (HER2), and Progesterone Receptor (PR).[44] TNBCs are characterized by high metastasis, chemo-resistance, and poor prognosis with a lower five-year survival rate relative to all the other non-TNBCs.[45] Currently, there are no efficient targeted treatment options for TNBC. Therefore, identification of new drug candidates for TNBC is urgently warranted.

STAT3 plays a critical role in TNBCs, as it regulates several genes vital to cell survival, metastasis, and invasiveness.[46] Constitutive activation of STAT3 in MDA-MB-231 cells promotes cell survival by regulating the expression of Bcl-2, Bcl-xL, Survivin, cyclin D1, c-Myc, and Mcl-1.[47] Conversely, A549 and MCF-7 cell lines have very low levels of constitutively active STAT3.[48-53]Due to their combined effect on inhibition of STAT3 pathway, PYM-HDACi compounds are expected to be more cytotoxic to STAT3-dependent cells such as MDA-MB-231 while somewhat less toxic to cell lines, such as A549 and MCF-7, with low levels of constitutively active STAT3.

We observed that the two classes of the PYM-HDACi compounds have distinct effects on the viability of the cell lines tested. Class I compounds **12a-c** showed preferential cytotoxicity to

the STAT3-dependent MDA-MB-231 cells with linker-length-dependent potency that also closely tracks with their HDAC inhibition potency. Specifically, compound **12a** is only cytotoxic to MDA-MB-231 with an IC_{50} of 38.38 ± 1.0 μM. In addition to being more potent than **12a** against MDA-MB-231, compounds **12b** and **12c** are also cytotoxic toward A549 and MCF-7 cells. However, **12b** and **12c** displayed >3-5-fold selectivity for MDA-MB-231 relative to the other tested cell lines (Table 2). By testing the intermediate ester **12d**, we subsequently confirmed that the modification that we introduced did not abolish the independent antiproliferative effect of PYM. In fact, compound **12d** is 2.5-4.6-fold more potent than PYM against the two cell lines for which PYM IC_{50}s were measurable within the concentration range we used (Table 2).

Presumably, due to its poor HDAC inhibitory activity and/or high hydrophilicity (CLogP = 0.877) which may negatively impact cell penetration, compound **18** did not show anti-proliferative activity towards all the cell lines tested. The additional phenyl ring in compound **23**, which resulted in the enhancement of its HDAC6 inhibition activity relative to **18** and higher hydrophobicity (CLogP = 2.765), also results in it having broad antiproliferative activities against the tested cell lines. However, **23** displayed little or no cell line selectivity (Table 2) which suggests that its antiproliferative activity may be largely due to HDAC inhibition. Although all the PYM-HDACi compounds are less potent relative to SAHA, the control HDACi, the selectivity of the class I compounds **12a-c** toward STAT3-dependent MDA-MB-231 suggest the contribution of the inhibition of STAT3 pathway to the anti-proliferative activities of these compounds since most non-targeted HDACi are incapable of tumor cells selectivity, a cause of their off-target toxic effects.[20] Interestingly, a combination therapy experiment whereby we used fixed concentration of of PYM (100 μM, approx ½ IC_{50} against MDA-MB-231 cells) and varying the concetrations of SAHA showed only slight to moderate improvements in the potency, relative to SAHA as a standalone agent, against all cell lines tested, including the non-transformed Vero cells. This combination did not result in MDA-MB-231 cell-selectivity that we noticed in the designed mutiple ligands PYM-HDACi **12b** and **12c**.

Table 2. Anti-proliferative activity of PYM-HDACi compounds (IC_{50} in μM).

Compound	A549	MCF-7	MDA-MB-231	VERO
12a	NI	NI	38.38± 1.0	ND
12b	65.49 ± 4.6	57.33 ± 3.4	12.20 ± 2.2	40.25 ± 3.58
12c	88.46 ±10.5	83.34 ± 15.5	21.4 ± 3.7	NI
12d	113.75 ± 3.95	96.6 ± 6.85	94.93 ± 9.67	112.65 ± 8.15
18	NI	NI	NI	ND
23	10.00 ± 1.92	9.3 ± 1.6	5.43 ± 1.2	6.9 ± 0.4
PYM	NI	453	238	NI
SAHA	15.73 ± 0.99	3.49 ± 0.05	3.40 ± 0.20	4.465 ± 0.68
PYM + SAHA	10.19 ± 0.87	2.29 ± 0.46	1.865 ± 0.48	1.305 ± 0.12

*Each value is obtained from a duplicate of three simultaneous experiments. NI: No Inhibition. ND: Not Determined at a maximum concentration of 100 μM. Comb. means SAHA with variable concentration combined with 100μM PYM

Intracellular Target Validation

To determine the contributions of HDAC and STAT3 pathway inhibition to the antiproliferative activities of PYM-HDACi compounds, we used immunoblotting to investigate the MDA-MB-231 cells response to one of the lead compounds **12c** using SAHA and PYM as positive controls for HDAC and STAT3 inhibition respectively. For HDAC inhibition, we monitored histone 4 (H4) and tubulin acetylation states as markers for HDACs 1 and 6 intracellular inhibition activities, respectively.[54,55] GAPDH expression was used as a protein loading control. When exposed to the cells at ½-IC_{50}, IC_{50} and 2x-IC_{50}, **12c** induced accumulation of acetylated H4 and acetylated tubulin. Similarly, SAHA at 1.5μM induced H4 and tubulin hyperacetylation (Figure 7). PYM has no effect on the acetylation status of tubulin and H4. This result strongly suggests that the PYM-HDACi **12c** inhibits these HDACs intracellularly, an attribute which contributes to their antiproliferative activity.

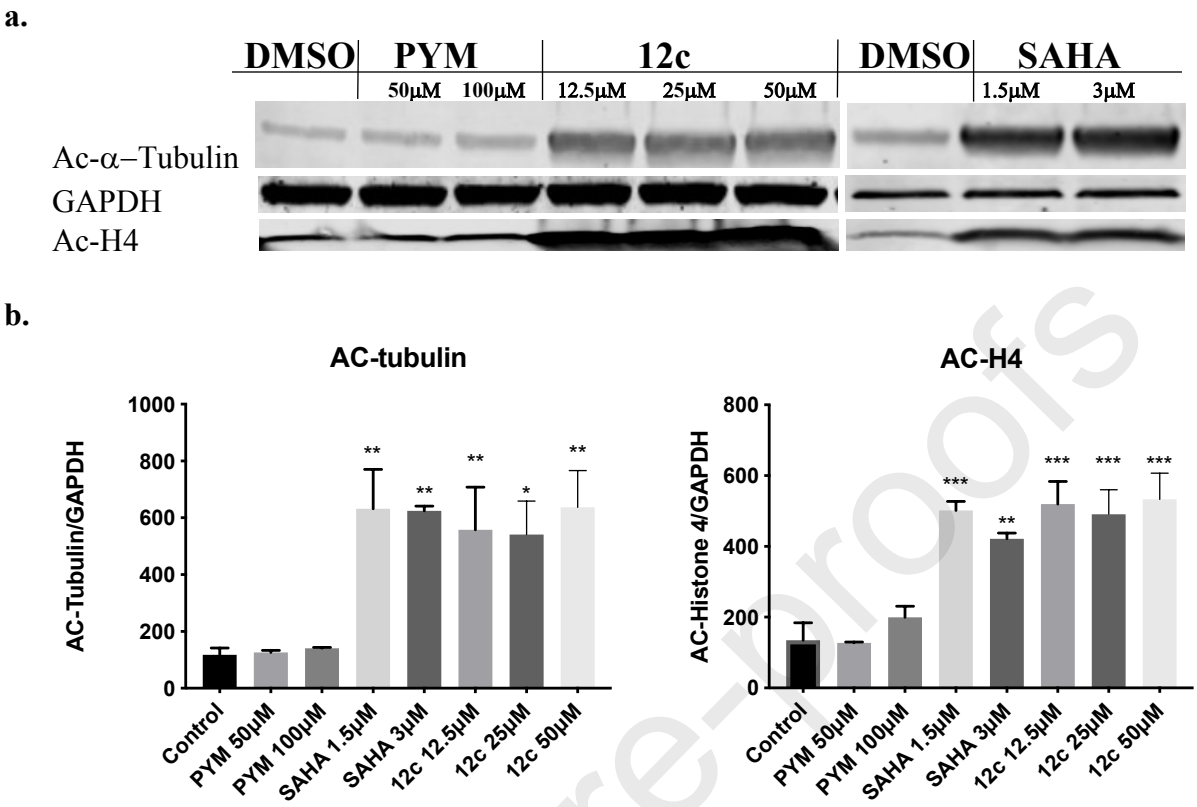

Figure 7. The Western blot analysis. (a) Immunoblotting of the acetylation status of tubulin and H4 of MDA-MB-231 treated with DMSO, PYM, SAHA, and **12c** for 4 h. Cells were serum-starved 24 h prior to the treatment. Acetylated α–tubulin and acetylated H4 are upregulated by SAHA and **12c** but not PYM. (b) Quantification of acetylated α–tubulin and acetylated H4 obtained by averaging data from two independent experiments. (Bars show mean plus standard deviation; * $P < 0.05$; ** $P < 0.0021$;***$P<0.0002$)

To elucidate the effect of the PYM-HDACi compounds on the STAT3 pathway, we probed the effects of **12c**, SAHA and PYM on the intracellular expression of STAT3, pSTAT3, p38, p-p38, Bcl-2, and Bcl-xL. Bcl-2 and Bcl-xL are anti-apoptotic genes whose expressions are upregulated by constitutive activation of STAT3.[56-58] Conversely, inhibition of STAT3 upregulates the intracellular level of p-p38.[59-61] As stated earlier, HDACi inhibits STAT3 pathway through direct downregulation of pSTAT3. The exact mechanism of the inhibition of

the STAT3 pathway by PYM has not been fully elucidated. However, it has been recently shown that PYM is a direct inhibitor of STAT3 transcriptional activity as PYM could upregulate pSTAT3 cellular levels while downregulating the expression of pSTAT3 target genes, including Bcl-2 and Bcl-xL, in TNBC cell lines.[62] We observed that **12c** (at 1/4th-, ½- and 1x-IC_{50}) and SAHA (at 1/4th- and ½-IC_{50}) caused concentration-dependent upregulation of p-p38 and downregulation of Bcl-xL in MDA-MB-231 cells. Within this concentration range, **12c** slightly downregulates Bcl-2 levels while SAHA caused no statistically relevant changes to the intracellular levels of Bcl-2. PYM (at 50 μM and 100 μM) has a similar effect as SAHA, causing concentration-dependent upregulation of p-p38 and Bcl-xL and no effect on Bcl-2 levels (Figures 8a and 8b). Interestingly, the effects of **12c** and PYM on pSTAT3 levels are closely aligned as they both caused upregulation of pSTAT3 while SAHA cause a slight downregulation of pSTAT3. The observed PYM-induced upregulation of pSTAT3 is in agreement with a previous observation.[62] To further confirm this effect on STAT3 pathway, we investigated the effects of **12c**, SAHA and PYM on the intracellular levels of the cyclin D1, a downstream protein of STAT3 pathway.[47] We observed that cyclin D1is significantly downregulated with **12c**, SAHA and PYM at approx. ½ - and 1x-IC_{50} concentration (Figures 9a and 9b). Collectively, this data suggests that the intracellular inhibitions of HDACs and the STAT3 pathway contribute to the anti-proliferative activity of the PYM-HDACi compounds **12c**. However, the mechanism of STAT3 pathway inhibition of **12c** is distinct from that of prototypical HDACi and very similar to that of STAT3 inhibitor template PYM. This distinction could be the basis for the TNBC cell selectivity of the PYM-HDACi.

a.

DMSO	**PYM**		**12c**			SAHA	
	50μM	100μM	5μM	12.5μM	25μM	0.8μM	1.6μM

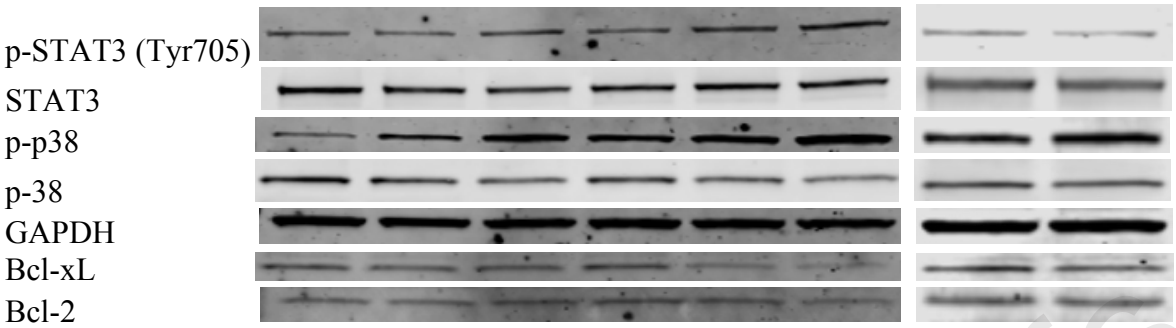

b.

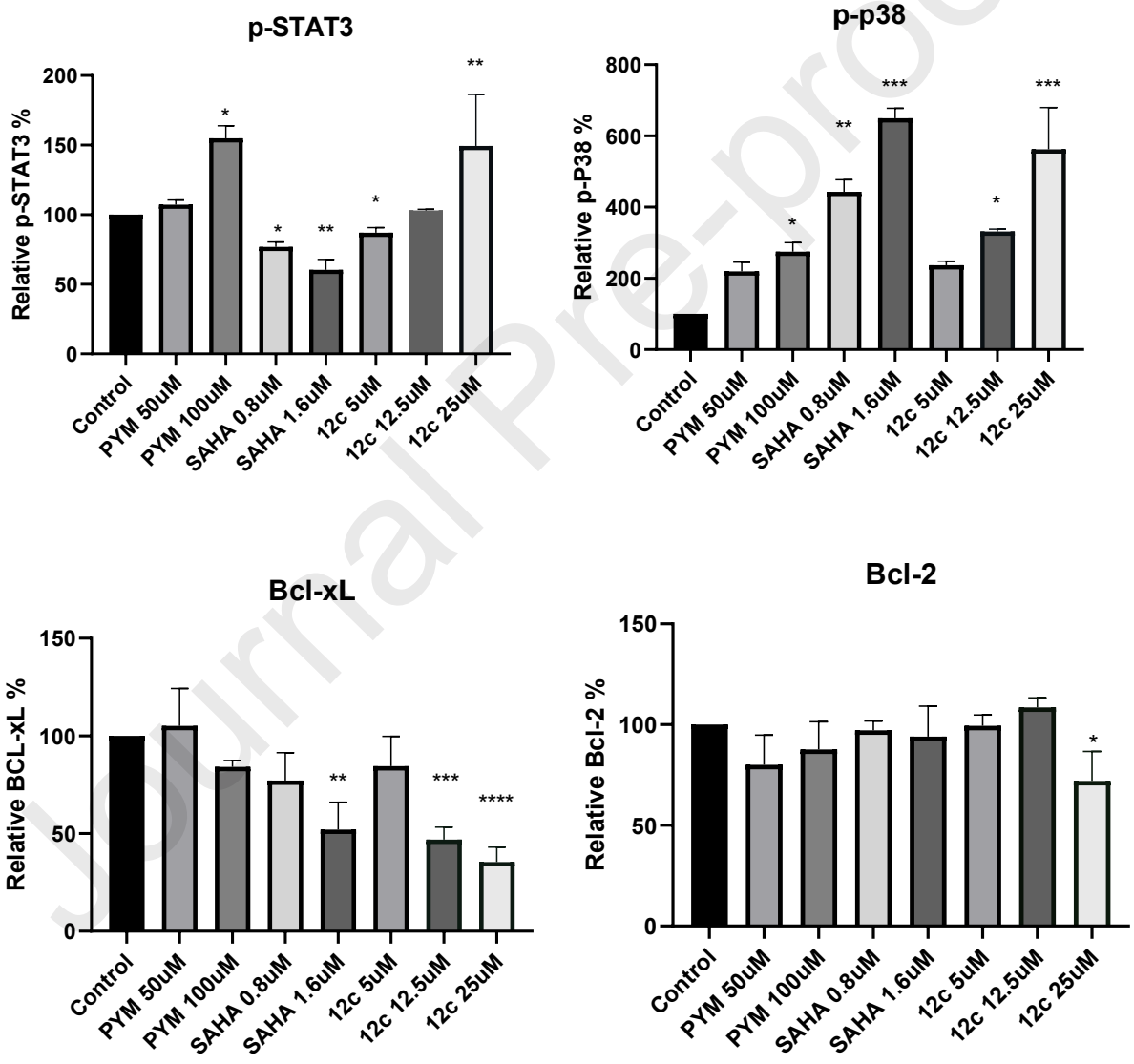

Figure 8. (a) Western blot analysis of the effects of compounds on the STAT3 pathway in MDA-MB-231 cells. Cells were serum-starved for 24 h prior to treatment with the tested agents such that the final DMSO content in the media is 0.1%. Cells were treated with the tested agents for 24 h. Images show the effects of DMSO, PYM, **12c** and SAHA on the intracellular levels of selected STAT3 pathway markers. (b) Quantification of the Western blots data probing for the effects of PYM, SAHA, and **12c** on the STAT3 pathway in MDA-MB-231 cells. (Bars show mean plus standard deviation; * P < 0.05; ** P < 0.0021; ***P<0.0002).

a.

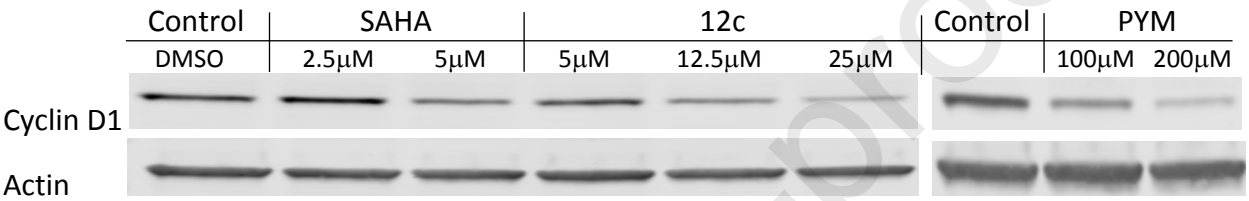

b.

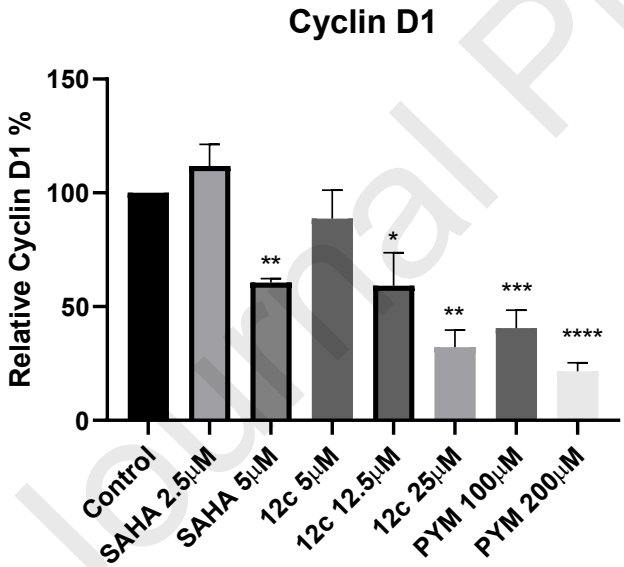

Figure 9. (a) Western blot analysis and (b) quantification of the Western blots data revealed the effects of **12c** on the cyclin D1 expression MDA-MB-231 cells. Experimental conditions are the same for the data shown in Figure 8. (Bars show mean plus standard deviation; * P < 0.05; ** P < 0.0021;***P<0.0002; ****P<0.00001).

Flow Cytometry for Cell Cycle Analysis.

We then performed cell cycle analysis to determine the effects of PYM-HDACi **12c**, **12b** and SAHA on MDA-MB-231 cell cycle distribution. We observed that the effects of **12c** (12.5 and 25 μM), **12b (15**μM) and SAHA (5 μM) on cell cycle are very similar as they induced significant G2 phase arrest (Figure 10 and Figure S2). Previous studies have shown that SAHA caused G2 arrest when exposed to breast cancer cells at concentrations above 3.0 μM.[63] The G2 cell cycle arrest induced by these compounds suggests that in addition to their cytotoxicity effects, they also induce MDA-MB-231 cell apoptosis.

A.

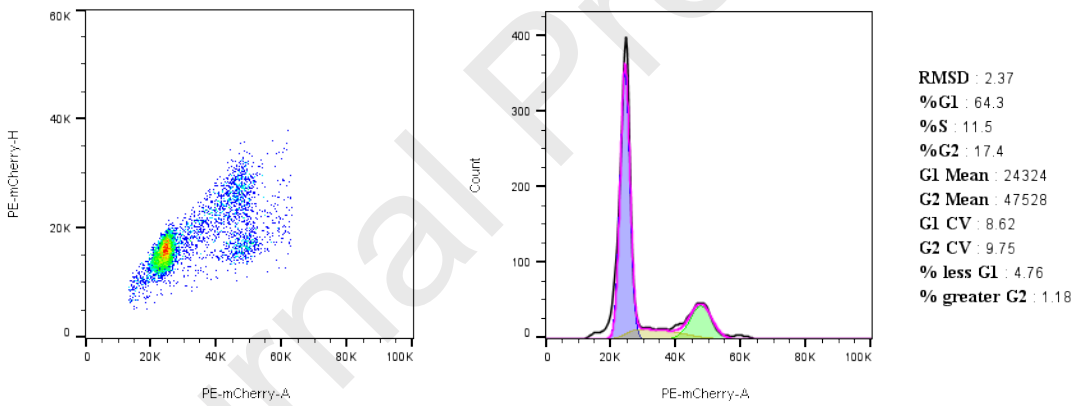

B.

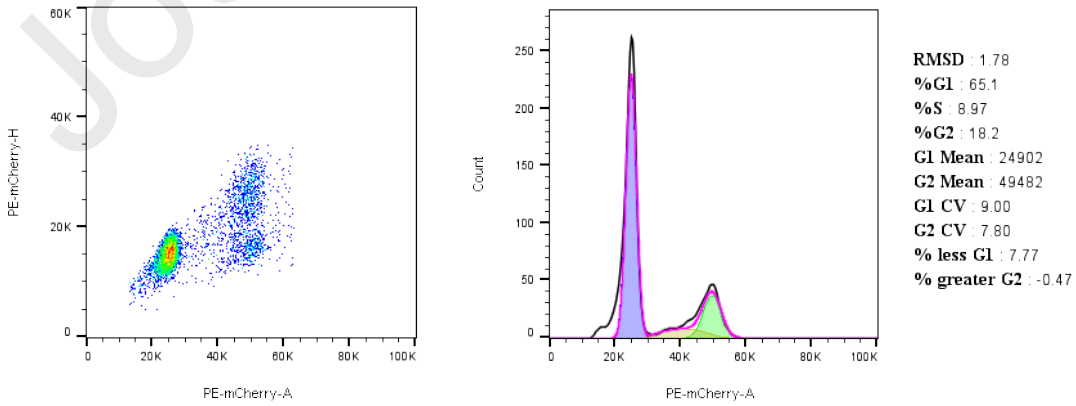

C.

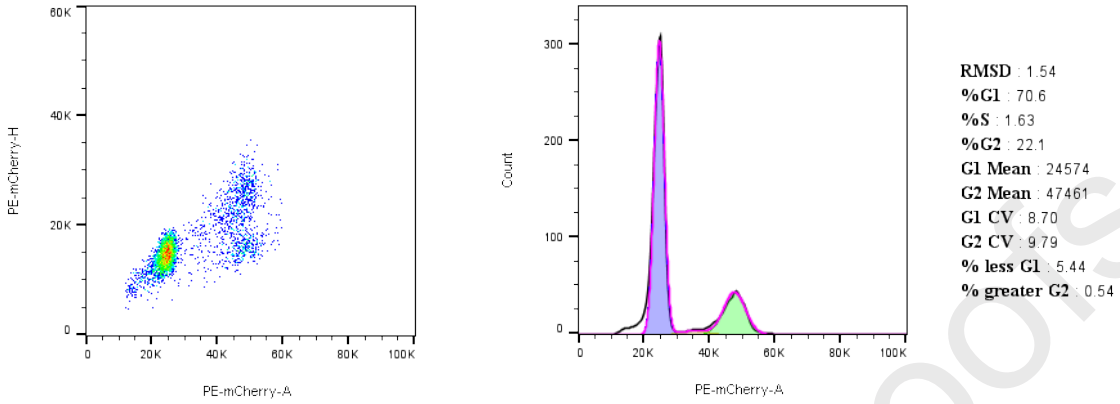

D.

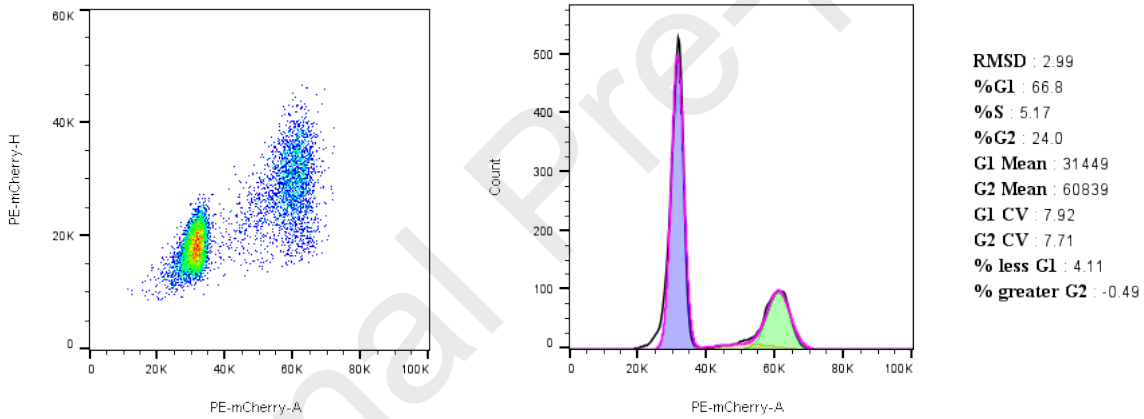

Figure 10. Effect of (a) DMSO control, (b) **12c** (12.5μM), (c) **12c** (25μM), and (d) SAHA (5μM) on MDA-MB-231 cell cycle progression.

Conclusion

We disclosed in this study two classes of dual-acting compounds designed to inhibit HDACs and the STAT3 pathway. We observed that the class I PYM-HDACi compounds **12a-c** potently inhibit HDACs 1 and 6 in cell-free assays and are preferentially cytotoxic to MDA-MB-231, a TNBC cell line that is highly STAT3-dependent. Moreover, target validation studies revealed that a representative compound **12c** elicited a signature of HDAC and STAT3 pathway inhibition intracellularly. In addition, **12b** and **12c** show significant selective cell cytotoxicity to TNBC. Overall, these compounds show promise as leads to develop targeted therapy for TNBC.

Experimental section

Materials and methods

4-Bromophenyl acetonitrile, ethyl propionate, O-tritylhydroxylamine, methyl acrylate, were purchased from Sigma-Aldrich. Trimethylsilylacetylene was purchased from Alfa Aesar. All commercially available starting materials were used without purification. Reaction solvents were high performance liquid chromatography (HPLC) grade or American Chemical Society (ACS) grade and used without purification. Analtech silica gel plates (60 F254) were used for analytical TLC, and Analtech preparative TLC plates (UV 254, 2000 μm) were used for purification. UV light and anisaldehyde/iodine stain were used to visualize the spots. 200-400 Mesh silica gel was used in column chromatography. Nuclear magnetic resonance (NMR) spectra were recorded on a Varian-Gemini 400 MHz, Bruker 500 MHz or 700 MHz magnetic resonance spectrometer. ^{1}H NMR Spectra were recorded in parts per million (ppm) relative to the residual peaks of $CHCl_3$ (7.24 ppm) in $CDCl_3$ or CHD_2OD (4.78 ppm) in CD_3OD or DMSO-d_5 (2.49 ppm) in DMSO-d_6. ^{13}C spectra were recorded relative to the central peak of the $CDCl_3$ triplet (77.0 ppm) or CD_3OD

septet (49.3 ppm) or DMSO-d_6 septet (39.7 ppm) and were recorded with complete hetero-decoupling. Original 'fid' files were processed using MestReNova LITE (version 5.2.5-5780) program. High-resolution mass spectra were recorded at the Georgia Institute of Technology mass spectrometry facility in Atlanta.

2-(4-Bromophenyl)-3-oxopentanenitrile (**3**). To a solution of 4-bromophenyl acetonitrile **1** (1.4 g, 7 mmol) in THF (10 mL), potassium tert-pentylate **2** (25% in toluene) (12.2 mL, 21 mmol) was added dropwise, followed by addition of ethyl propionate. The reaction mixture was stirred for 20 min, and then neutralized (approx. pH=7) with 1N HCl to. Water (5 mL) and EtOAc (10 mL) were added and the two layers separated. The organic layer was washed with water (10 mL) and brine (10 mL) and dried over Na_2SO_4. The crude was purified by column chromatography on silica gel, eluting with Hexanes:EtOAc 4:1, to furnish compound **3** (1.6 g, 90%) as yellow oil. ^{1}H NMR (400 MHz, CD_3OD) δ 7.62 – 7.53 (m, 2H), 7.49 – 7.41 (m, 2H), 2.71 – 2.55 (m, 2H), 1.31 – 1.23 (m, 3H). ^{13}C NMR (101 MHz, CD_3OD) δ 173.5, 132.1, 131.9, 130.9, 130.0, 129.0, 120.0, 119.4, 85.6, 28.8, 11.2. HRMS (ESI) m/z Calcd. for $C_{11}H_{10}NO$ Br [$M+H^+$]: 250.9946, found 250.9946.

2-(4-Bromophenyl)-3-methoxypent-2-enenitrile (**5**). A mixture of compound **3** (3.1 g, 12.5 mmol) and trimethyl orthoacetate **4** (12.3 mL, 96.5 mmol) was heated at 107 °C for 6 h. Dichloromethane (DCM) (15mL) was added and the mixture was washed with water (15 mL), $NaHCO_3$ (15 mL), and brine (15 mL). The organic layer was dried over Na_2SO_4 and the crude was purified by column chromatography on silica gel, eluting with Hexanes:EtOAc 3:1, to furnish compound **5** (1.1 g, 33%) as yellow oil. ^{1}H NMR (400 MHz, $CDCl_3$) δ 7.57 – 7.35 (m,

4H), 2.77 (q, J = 7.6 Hz, 2H), 1.32 – 1.26 (m, 3H). ^{13}C NMR (101 MHz, $CDCl_3$) δ 173.1, 131.4, 130.8, 129.8, 120.7, 119.7, 91.5, 56.4, 24.1, 12.8. HRMS (ESI) m/z Calcd. for $C_{12}H_{12}NO$ Br [M+H$^+$]: 265.0102, found 265.0103.

5-(4-Bromophenyl)-6-ethylpyrimidine-2,4-diamine (**6**). A mixture of compound **5** (846 mg, 3.2 mmol), sodium hydrogen carbonate (588 mg, 7mmol) and guanidine hydrochloride (668 mg, 7 mmol) in dry DMSO (10 mL) was heated at 100 °C for 5 h. To the reaction was added 10% MeOH in DCM (30 mL) and the mixture was washed with water (3× 15 mL) and brine (15 mL) The organic layer was dried over Na_2SO4, concentrated and the concentrate was purified by precipitation with EtOAc to furnish compound **6** (670 mg, 72%) as a white powder. ^{1}H NMR (400 MHz, CD_3OD) δ 7.62 (d, J = 8.5 Hz, 2H), 7.16 (d, J = 8.5 Hz, 2H), 2.22 (q, J = 7.6 Hz, 2H), 1.03 (t, J = 7.6 Hz, 3H). ^{13}C NMR (101 MHz, DMSO-d_6) δ 166.8, 162.6, 162.4, 135.9, 133.4, 132.3, 121.0, 105.9, 49.1, 27.9, 13.7. HRMS (ESI) m/z Calcd. for $C_{12}H_{14}N_4Br$ [M+H$^+$]: 293.0396, found for 293.0399.

Di-tert-butyl (5-(4-bromophenyl)-6-ethylpyrimidine-2,4-diyl)bis((tert-butoxycarbonyl) carbamate) (**7**). Compound **6** (104.4 mg, 0.3 mmol) and DMAP (4.3 mg, 0.03 mmol) were dissolved in THF (5 mL) and flushed with argon. Boc_2O (622.7 mg, 2.8 mmol) was added to the solution and thereaction was stirred overnight at 40 °C. The mixture was partitioned between water (15 mL) and DCM (25 mL), the organic layer was separated, washed with brine (15 mL) and dried over Na_2SO_4. The crude was purified on preparative TLC eluting with Hexanes:EtOAc 4:1 to yield compound **7** (204 mg, 86% conversion) as a yellow oil. ^{1}H NMR (400 MHz, $CDCl_3$) δ 7.56 – 7.48 (m, 2H), 7.14 – 7.03 (m, 2H), 2.59 (q, J = 7.5 Hz, 2H), 1.42 (s,

18H), 1.31 (s, 18H), 1.13 (t, *J* = 7.5 Hz, 3H). ^{13}C NMR (101 MHz, $CDCl_3$) δ 173.9, 158.6, 157.4, 150.3, 149.8, 132.0, 131.7, 130.8, 128.3, 122.6, 83.5, 83.1, 28.4, 27.9, 13.0. HRMS (ESI) m/z Calcd. for $C_{32}H_{46}O_8N_4Br$ [M+H$^+$]: 693.2494, found 693.2493.

Di-tert-butyl (6-ethyl-5-(4-((trimethylsilyl)ethynyl)phenyl)pyrimidine-2,4-diyl)bis((tert-butoxycarbonyl)carbamate) **(9).** Compound **7** (315 mg, 0.4 mmol), $Pd(PPh_3)_4$ (26 mg, 0.02 mmol), and CuI (8.6 mg, 0.04 mmol) were dissolved in acetonitrile (5 mL) under argon. Trimethylsilylacetylene **8** (0.1 mL, 0.9 mmol) was added, followed by Hunig's base (0.2 mL, 0.9 mmol). The reaction mixture was heated at 75 °C overnight. The mixture was partitioned between water (15 mL) and DCM (25 mL). The organic layer was separated, washed with brine (5 mL) and dried over Na_2SO_4. Crude product **9** was used in the next step without purification.

Di-tert-butyl (6-ethyl-5-(4-ethynylphenyl)pyrimidine-2,4-diyl)bis((tert-butoxycarbonyl)carbamate) (**10**). Potassium carbonate (74 mg, 0.5 mmol) was added to a solution of crude compound **9** (190 mg) in methanol (3 mL). The reaction mixture stirred for 2 h at room temperature. The mixture was partitioned between water (10 mL) and DCM (20 mL). The organic layer was separated, washed with brine (10 mL), and dried over Na_2SO_4. The crude was purified on preparative TLC eluting with Hexanes:EtOAc:Ether 8:1:1 to furnish compound **10** (93 mg, 36% overall yield two steps starting from **7**) as a white powder. ^{1}H NMR (400 MHz, $CDCl_3$) δ 7.57 – 7.49 (m, 2H), 7.25 – 7.18 (m, 2H), 3.14 (s, 1H), 2.61 (dt, *J* = 7.5, 6.0 Hz, 2H), 1.45 (s, 18H), 1.34 (s, 18H), 1.17 (q, *J* = 7.6 Hz, 3H). ^{13}C NMR (101 MHz, $CDCl_3$) δ 173.8, 158.7, 157.1, 150.9, 150.0, 134.0, 132.3, 129.5, 128.8, 122.4, 83.8, 83.5, 83.1, 78.4, 28.5, 27.7, 13.0. HRMS (ESI) m/z Calcd. for $C_{34}H_{47}O_8N_4$ [M+H+]: 639.3388, found 639.3382.

6-ethyl-5-(4-ethynylphenyl)pyrimidine-2,4-diamine (**10a).** Potassium carbonate (37 mg, 0.25 mmol) was added to a solution of crude compound **9** (95 mg, 0.13mmol) in methanol (3 mL). The reaction mixture stirred for 2 h at room temperature. The mixture was partitioned between water (10 mL) and DCM (20 mL). The organic layer was separated, washed with brine (10 mL), and dried over Na_2SO_4. The crude was purified on preparative TLC eluting with Hexanes:EtOAc:Ether 8:1:1 to furnish compound **10** (63 mg, 75%) as a white powder. The product was added to TFA (2 mL) for a neat deprotection of the Boc group at ambient temperature for 4-8h. The TFA solution was neutralized with sodium bicarbonate and the mixture partitioned between water (30 mL) and DCM (50 mL). The two layers were separated, the organic layer was dried over Na_2SO_4 and the solvent evaporated off. The crude product was purified by silica gel column chromatography, eluting with DCM: MeOH=10:1, to give **10a** as solid, 19 mg (yield 81%). ^{1}H NMR (400 MHz, DMSO-d_6) δ 7.51 (d, J=8.3 Hz, 2H), 7.19 (d, J=8.3 Hz, 2H), 4.22 (d, J = 0.8 Hz, 1H), 2.09 (q, J = 7.5 Hz, 2H), 1.17 – 0.73 (t, J=7.6 Hz 3H). HRMS (ESI) m/z Calcd. for $C_{14}H_{14}N_4$ [M+H+]: 239.1287, found 239.1291

6-(4-(4-(2,4-Diamino-6-ethylpyrimidin-5-yl)phenyl)-1H-1,2,3-triazol-1-yl)-N-hydroxyhexanamide (**12a**). Compound **10** (41 mg, 0.06 mmol) and 4-azido-N-(trityloxy)hexanamide **11a** (32 mg, 0.08 mmol) were dissolved in anhydrous THF (5 mL) and purged with argon for 15 min. Copper (I) iodide (6 mg, 0.03 mmol) and Hunig's base (0.02 mL, 0.1 mmol) were added, the mixture was purged with argon for additional 15 min and stirring continued for approx. 12 h. The reaction was partitioned between DCM (20 mL) and sat. NH_4Cl/

conc. NH_4OH (4:1) (15 mL) and the two layers separated. The organic layer was washed with sat. NH_4Cl/ conc. NH_4OH (4:1) (2 x 15 mL), sat. brine (15 mL), dried over Na_2SO_4 and the solvent was evaporated off. The crude was then dissolved in DCM: TFA (1: 0.2 mL) andtriisopropyl silane was added dropwise until the color transformed from dark yellow to pale yellow. TLC indicated the complete consumption of the starting material after 1 h. Solvent was evaporated off and the crude product was purified by precipitation in EtOAc to give the title compound (23 mg, 88%) as a pale yellow solid. ^{1}H NMR (500 MHz, CD_3OD) δ 8.46 (s, 1H), 8.02 (d, J = 7.7 Hz, 2H), 7.40 (dd, J = 15.1, 8.0 Hz, 2H), 4.50 (d, J = 6.2 Hz, 2H), 2.42 (q, J = 7.2 Hz, 2H), 2.21 – 2.04 (m, 2H), 2.02 (s, 2H), 1.71 (s, 2H), 1.41 (s, 2H), 1.21 – 1.12 (m, 3H). ^{13}C NMR (126 MHz, CD_3OD) δ 165.2, 155.5, 154.6, 146.9, 131.6, 130.9, 126.7, 121.4, 108.8, 71.2, 50.1, 29.8, 29.2, 25.6, 24.6, 23.9, 17.3, 11.8. HRMS (ESI) m/z Calcd. for $C_{20}H_{27}O_2N_8$ [M+H$^+$]: 411.2251, found 411.2246.

7-(4-(4-(2,4-Diamino-6-ethylpyrimidin-5-yl)phenyl)-1H-1,2,3-triazol-1-yl)-N-hydroxyheptanamide (**12b**). The reaction of compound **10** (40 mg, 0.06 mmol), 4-azido-N-(trityloxy)heptanamide **11b** (32 mg, 0.08 mmol), copper (I) iodide (6 mg, 0.03 mmol) and Hunig's base (0.02 mL, 0.1 mmol) in anhydrous THF (5 mL) as described for the synthesis **12a** furnished the title compound **12b**. ^{1}H NMR (400 MHz, CD_3OD) δ 8.43 (s, 1H), 7.99 (d, J = 6.4 Hz, 2H), 7.37 (s, 2H), 4.47 (s, 2H), 2.39 (s, 2H), 2.19 (d, J = 31.3 Hz, 2H), 1.99 (d, J = 11.8 Hz, 2H), 1.60 (s, 2H), 1.38 (s, 4H), 1.14 (d, J = 6.1 Hz, 3H). ^{13}C NMR (101 MHz, CD_3OD) δ 164.9, 155.4, 154.8, 146.7, 131.4, 130.9, 130.6, 126.5, 121.4, 108.8, 50.1, 29.8, 29.4, 28.1, 26.1, 25.0, 23.7, 23.0, 11.8. HRMS (ESI) m/z Calcd. for $C_{21}H_{29}O_2N_8$ [M+H+]: 425.2408, found 425.2402.

8-(4-(4-(2,4-Diamino-6-ethylpyrimidin-5-yl)phenyl)-1H-1,2,3-triazol-1-yl)-N-hydroxyoctanamide (**12c**). The reaction of compound **10** (110 mg, 0.16 mmol), 4-azido-N-(trityloxy)heptanamide **11c** (100 mg, 0.22 mmol), copper (I) iodide (20 mg, 0.1 mmol) and Hunig's base (0.2 mL, 1.17 mmol) in anhydrous THF (5 mL) as described for the synthesis **12a** furnished the title compound 12c. 1H NMR (700 MHz, DMSO-*d*6) δ 12.40 (s, 1H), 10.31 (s, 1H), 8.66 (s, 1H), 8.14 (s, 1H), 7.95 (d, *J* = 8.0 Hz, 2H), 7.61 (s, 2H), 7.33 (d, *J* = 7.9 Hz, 2H), 6.87 (s, 1H), 2.25 (q, *J* = 7.6 Hz, 2H), 1.88 (dt, *J* = 24.4, 7.2 Hz, 4H), 1.45 (t, *J* = 7.5 Hz, 2H), 1.24 (d, *J* = 17.7 Hz, 6H), 1.13 – 0.75 (m, 5H). ^{13}C NMR (176 MHz, DMSO) δ 169.5, 164.6, 155.2, 154.7, 146.3, 131.5, 130.9, 126.5, 122.1, 108.5, 65.4, 50.0, 32.6, 30.1, 28.9, 28.5, 26.2, 25.5, 24.1, 18.3, 15.6, 13.1. HRMS (ESI) m/z Calcd. for $C_{21}H_{29}O_2N_8$ [M+H+]: 439.2564, found 439.2558.

Ethyl 8-(4-(4-(2,4-diamino-6-ethylpyrimidin-5-yl)phenyl)-1H-1,2,3-triazol-1-yl)octanoate (**12d).** A mixture of compound **10a** (20 mg, 0.084 mmol), ethyl 8-azidooctanoate **11d** (50 mg, 0.11 mmol), copper (I) iodide (5 mg, 0.026 mmol) and Hunig's base (0.2 mL, 1.17 mmol) in anhydrous THF (3 mL) was purged with argon for 15 min and the reaction was kept stirring for approx. 12 h. The reaction was partitioned between DCM (20 mL) and sat. NH_4Cl/ conc. NH_4OH (4:1) (15 mL) and the two layers separated. The organic layer was washed with sat. NH_4Cl/conc. NH_4OH (4:1) (2 x 15 mL), sat. brine (15 mL), dried over Na_2SO_4 and the solvent was evaporated off. The product was purified by prep-TLC plate with EtOAc:MeOH=9:1. ^{1}H NMR (700 MHz, $CDCl_3$) δ 7.92 (d, *J* = 8.2 Hz, 2H), 7.81 (s, 1H), 7.32 (d, *J* = 8.2 Hz, 2H), 5.00 (s, 2H), 4.65 (s, 2H), 4.43 (t, *J* = 7.2 Hz, 2H), 4.13 (q, *J* = 7.1 Hz, 2H), 2.34 (q, *J* = 7.6 Hz, 2H),

2.29 (t, J = 7.5 Hz, 2H), 2.11 – 2.06 (m, 1H), 2.05 (s, 1H), 1.98 (t, J = 7.2 Hz, 2H), 1.63 (p, J = 7.4 Hz, 3H), 1.38 (q, J = 3.8 Hz, 4H), 1.34 (td, J = 6.5, 2.4 Hz, 1H), 1.31 – 1.22 (m, 7H), 1.09 (t, J = 7.5 Hz, 3H). ^{13}C NMR (176 MHz, $CDCl_3$) δ 173.7, 162.3, 147.2, 131.1, 130.3, 126.5, 119.5, 107.9, 76.9, 60.2, 50.4, 34.2, 30.3, 28.8, 28.7, 28.0, 26.3, 24.8, 14.3, 13.4. HRMS (ESI) m/z Calcd. for $C_{21}H_{29}O_2N_8$ [M+H+]: 452.2768, found 452.2758.

(E)-Methyl 3-(4-(2,4-diamino-6-ethylpyrimidin-5-yl)phenyl)acrylate (**14**). Compound **6** (90 mg, 0.3 mmol), methyl acrylate **13** (0.09 mL, 0.9 mmol), TEA (0.1 mL, 0.8 mmol), and tri-O-tolylphosphine (28 mg, 0.09 mmol) were dissolved in DMF (3 mL). The reaction mixture was purged with argon for 15 min, then Pd $(OAc)_2$ (10.3 mg, 0.05 mmol) was added, and the mixture was heated at 120 °C overnight. The reaction was partitioned between water (10 mL) and DCM (10 mL). The organic layer was separated, washed with brine (5 mL), and dried over Na_2SO_4. Solvent was evaporated off and the crude was purified on preparative TLC eluting with EtOAc:Hexanes:NEt_3 10:1:0.5 to yield compound **14** (50 mg, 55%) as a pale yellow powder. ^{1}H NMR (400 MHz, CD_3OD) δ 7.74 (d, J = 8.2 Hz, 3H), 7.32 (d, J = 7.7 Hz, 2H), 6.60 (d, J = 16.2 Hz, 1H), 2.38 – 2.21 (m, 2H), 1.10 (t, J = 7.4 Hz, 3H). ^{13}C NMR (101 MHz, CD_3OD) δ 167.4, 164.1, 157.7, 144.1, 134.6, 134.2, 130.9, 128.7, 118.6, 107.9, 70.3, 51.1, 31.8, 29.2, 25.4, 12.0. HRMS (ESI) m/z Calcd. $C_{16}H_{19}O_2N_4$ [M+H$^+$]: 299.1503, found 299.1503.

(E)-Methyl 3-(4-(2,4-bis(bis(tert-butoxycarbonyl)amino)-6-ethylpyrimidin-5-yl)phenyl)acrylate (**15**). Compound **14** (27 mg, 0.09 mmol) and DMAP (1.1 mg, 0.009 mmol) were dissolved in THF (3 mL) and flushed with argon. Boc_2O was added to the solution and the mixture was

stirred overnight at 40 °C. The reaction was partitioned between water (10 mL) and DCM (20 mL) and the organic layer was separated, washed with brine (10 mL), and dried over Na_2SO_4. Solvent was evaporated off and the crude was purified on preparative TLC eluting with Hexanes:EtOAc 3:1 to yield compound **15** (35 mg, 56%) as a white solid. ^{1}H NMR (400 MHz, CD_3OD) δ 7.77 (s, 1H), 7.74 (d, *J* = 7.0 Hz, 2H), 7.34 (dd, *J* = 17.5, 8.2 Hz, 2H), 6.63 (dd, *J* = 16.1, 10.6 Hz, 1H), 3.80 (s, 3H), 2.80 – 2.57 (m, 2H), 1.48 (s, 18H), 1.35 (d, *J* = 4.3 Hz, 18H), 1.19 (t, *J* = 7.5 Hz, 3H). ^{13}C NMR (101 MHz, $CDCl_3$) δ 173.8, 167.3, 158.6, 157.4, 150.9, 149.8, 143.8, 135.3, 134.5, 129.8, 128.0, 118.7, 82.2, 81.3, 70.4, 51.9, 51.8, 29.7, 29.0, 28.6, 28.2, 28.0, 27.9, 27.8, 27.7, 13.2, 12.9. HRMS (ESI) m/z Calcd. $C_{36}H_{51}O_{10}N_4$ [M+H$^+$]: 699.3600, found 699.3595.

(E)-3-(4-(2,4-Bis(bis(tert-butoxycarbonyl)amino)-6-ethylpyrimidin-5-yl)phenyl)acrylic acid (**16**). Compound **15** (60 mg, 0.08 mmol) was dissolved in 1,4-dioxane (3 mL) and added dropwise to an aqueous solution (3 mL) containing hydroxylamine (6 mg, 0.2 mmol) and sodium hydroxide (10.2 mg, 0.2 mmol) at room temperature and stirred for 12 h. The mixture was concentrated under vacuum to remove organic solvent. The aqueous solution was adjusted to pH=1 with 1N HCl. The resulting precipitate was collected by filtration and dried to give compound **16** (35 mg, 60%) as a pale yellow solid. ^{1}H NMR (400 MHz, $CDCl_3$) δ 7.70 (s, 1H), 7.60 – 7.52 (m, 2H), 7.27 (d, *J* = 5.2 Hz, 1H), 7.22 (d, *J* = 8.1 Hz, 1H), 6.54 (s, 1H), 2.62 (dq, *J* = 15.2, 7.5 Hz, 2H), 1.51 (d, *J* = 15.4 Hz, 6H), 1.50 – 1.44 (m, 12H), 1.32 (s, 18H), 1.24 (d, *J* = 3.9 Hz, 3H). ^{13}C NMR (101 MHz, $CDCl_3$) δ 174.3, 158.9, 158.2, 157.6, 156.7, 150.7, 150.5, 150.0, 130.0, 129.5, 128.8, 128.1, 125.5, 81.5, 29.7, 29.0, 28.6, 28.3, 28.0, 27.8, 27.7, 13.1, 12.9. HRMS (ESI) m/z Calcd. $C_{35}H_{49}O_{10}N_4$ [M+H$^+$]: 685.3443, found 685.3434.

(E)-3-(4-(2,4-Diamino-6-ethylpyrimidin-5-yl)phenyl)-N-hydroxyacrylamide (**18**). Compound **16** (35 mg, 0.05 mmol), EDCI (9.5 mg, 0.05 mmol) and HOBT (6.9 mg, 0.05 mmol) were dissolved in DCM (3 mL) at 0 °C. After stirring at 0 °C for 15 min, *O*-tritylhydroxylamine (20.6 mg, 0.07 mmol) and Hunig's base (0.03 mL, 0.15 mmol) were added, and the mixture stirred for 12 h at room temperature. The reaction was partitioned between water (10 mL) and DCM (20 mL) and the organic layer was separated, washed with brine, and dried over Na_2SO_4. Solvent was evaporated off, the crude was dissolved in DCM: TFA (1: 0.2 mL) and triisopropyl silane was added dropwise until the color transformed from dark yellow to pale yellow. TLC indicated a complete consumption of the starting material after 1 h. Solvent was evaporated off and the crude product was purified by precipitation with EtOAc to give the title compound (3.6 mg, 24%) as a pale yellow solid. ^{1}H NMR (500 MHz, CD_3OD) δ 7.75 (d, J = 7.4 Hz, 2H), 7.66 (d, J = 15.6 Hz, 1H), 7.37 (d, J = 6.9 Hz, 2H), 6.59 (d, J = 15.3 Hz, 1H), 2.38 (d, J = 7.4 Hz, 2H), 1.15 (t, J = 7.3 Hz, 3H). ^{13}C NMR (126 MHz, CD_3OD) δ 171.8, 165.2, 158.0, 155.3, 144.8, 135.7, 130.7, 128.7, 120.4, 29.6, 27.2, 23.9, 12.0. HRMS (ESI) m/z Calcd. $C_{15}H_{18}O_2N_5$ [M+H+]: 300.1455, found 300.1451.

Di-tert-butyl (6-ethyl-5-(4'-hydroxy-[1,1'-biphenyl]-4-yl)pyrimidine-2,4-diyl)bis(tert-butoxycarbonylcarbamate) (**19**). Compound **7** (500 mg, 0.72 mmol) was mixed with iodo phenol (200 mg, 0.91 mmol), copper (I) iodide (20 mg, 0.105 mmol), and Tetrakis(triphenylphosphine) palladium (0) (83 mg, 0.072 mmol) in a pressure tube. Acetonitrile (5 mL) was added to dissolve the solids; the reaction tube was filled with argon and heated to 75°C for 10 min. Hunig's base (0.5 ml, 2.92 mmol) was added and the reaction was stirred at 75°C overnight. Solvent was

evaporated off and the crude was purified on silica gel eluting with EtOAc:Hexanes 1:1 to furnish compound **19** (401 mg, 77.7%) as a pale yellow solid. ^{1}H NMR (400 MHz, $CDCl_3$) δ 7.69 (d, *J* = 8.5 Hz, 2H), 7.62 (d, *J* = 8.7 Hz, 2H), 7.41 (d, *J* = 8.5 Hz, 2H), 7.04 (d, *J* = 8.7 Hz, 2H), 2.82 (q, *J* = 7.9 Hz, 2H), 1.67 (s, 8H), 1.59 (s, 14H), 1.46 (s, 14H), 1.32 (t, *J* = 7.5 Hz, 3H).

4'-(2,4-Bis(bis(tert-butoxycarbonyl)amino)-6-ethylpyrimidin-5-yl)-[1,1'-biphenyl]-4-yl trifluoromethanesulfonate (**20**).

Compound **19** (200 mg, 0.28 mmol) was dissolved into DCM (10 mL). To the solution was added pyridine (0.7 mL, 8.66 mmol) and the mixture cooled to -20°C for 10 min with stirring under Argon. Trifluoromethanesulfonic anhydride (0.3 mL, 1.78 mmol) was added dropwise to the mixture with stirring which continued for 30 min. The reaction was quenched with water (100 mL) and DCM (30 mL) was added. The two layers were separated, the organic layer was dried over Na_2SO_4 and solvent was evaporated off to furnish compound **20** (211mg, 0.252mmol) as yellow solid. Compound **20** was analytically pure and used for the next reaction without purification. ^{1}H NMR (400 MHz, $CDCl_3$) δ 7.62 (d, *J* = 3.2 Hz, 2H), 7.59 (d, *J* = 2.9 Hz, 2H), 7.33 (d, *J* = 8.4 Hz, 2H), 7.28 (d, *J* = 8.8 Hz, 2H), 2.70 (q, *J* = 7.9 Hz, 2H), 1.59 (s, 8H), 1.48 (s, 14H), 1.35 (s, 14H), 1.20 (t, *J* = 7.5 Hz, 3H).

Di-tert-butyl (6-ethyl-5-(4'-vinyl-[1,1'-biphenyl]-4-yl)pyrimidine-2,4-diyl)bis(tert-butoxycarbonylcarbamate) (**21**). Compound **20** (200 mg, 0.24 mmol) and potassium vinyltrifluoroborate (130mg, 0.97mmol) were dissolved in DMF (20 mL). Tetrakis(triphenylphosphine) palladium (0) (80 mg, 0.07 mmol) and Cesium carbonate (315 mg, 0.96 mmol) were added to the mixture and the reaction heated to 80°C for 5 min. Subsequently,

water (1 mL) was added dropwise into the mixture with stirring until the solution turned clear. Stirring continued at 80°C and the reaction was complete after 3 h. The solution was cooled down and partitioned between water (100 mL) and DCM (30 mL). The two layers were separated and the aqueous layer was extracted with DCM (30mL). The combined organic layers was washed with water (100 mL), dried over Na_2SO_4 and solvent was evaporated of *in vacuo*. The mixture was purified with column chromatography with Ethyl acetate: Hexane=2:3. The furnish compound **21** was gained (120mg, 70 %) as yellow liquid. 1H NMR (400 MHz, $CDCl_3$) δ 7.66 (d, *J* = 8.4 Hz, 2H), 7.61 (d, *J* = 8.3 Hz, 2H), 7.53 (d, *J* = 8.3 Hz, 2H), 7.34 (d, *J* = 8.4 Hz, 2H), 6.79 (dd, *J* = 17.6, 10.9 Hz, 1H), 5.83 (d, *J* = 17.6 Hz, 1H), 5.32 (d, *J* = 11.6 Hz, 1H), 2.74 (t, *J* = 7.9 Hz, 2H), 1.51 (s, 18H), 1.37 (s, 18H), 1.23 (t, *J* = 7.5 Hz, 3H).

(E)-Di-tert-butyl (6-ethyl-5-(4'-(3-oxo-3-((trityloxy)amino)prop-1-en-1-yl)-[1,1'-biphenyl]-4-yl)pyrimidine-2,4-diyl)bis(tert-butoxycarbonylcarbamate) (**22**). Compound **21** (100 mg, 0.14 mmol), N-[Tris(hydroxymethyl)methyl]acrylamide (56 mg, 0.17 mmol) and Hoveyda-Grubbs 2nd generation catalyst (10 mg, 0.016 mmol) was added to the reaction flask and the mixture was dissolved in DCM (10 mL). The reaction mixture was heated under Argon atmosphere at 33°C overnight. The solution was evaporated and the crude was purified by preparative TLC eluting with EtOAc:Hexane 1:1 to furnish compound **22** (35mg , 23 %) as white solid. ^{1}H NMR (400 MHz, $CDCl_3$) δ 7.79 (d, *J* = 8.8 Hz, 2H), 7.73 (d, *J* = 8.3 Hz, 2H), 7.63 – 7.25 (m, 21H), 2.80 (q, *J* = 7.9 Hz, 2H), 1.60 (s, 18H), 1.47 (s, 18H), 1.35 (t, *J* = 7.5 Hz, 3H).

(E)-3-(4'-(2,4-Diamino-6-ethylpyrimidin-5-yl)-[1,1'-biphenyl]-4-yl)-N-hydroxyacrylamide (**23**). Compound **22** (35 mg, 0.032 mmol) was cooled to 0°C and mixed with TFA (2 mL) as a neat

reaction. The solution was stirred at room, triisopropylsilane (0.3-0.5 mL) was added until the bright yellow color vanished and stirring continued for 2 h. The solvent was evaporated by Rotovap and the residue was dried using high vacuum. The dried residue was washed by titurated with diethyl ether and a brown solid which crashed out was filtered to furnish compound **23** (8.8 mg, 72 %). ^{1}H NMR (400 MHz, DMSO-d_6) δ 10.81 (s, 1H), 9.09 (s, 1H), 8.32 (s, 1H), 7.84 (d, J = 22.8 Hz, 3H), 7.69 (s, 1H), 7.52 (d, J = 15.8 Hz, 1H), 6.52 (d, J = 15.8 Hz, 1H), 2.25 (q, J = 7.7 Hz, 2H), 1.07 (t, J = 7.5 Hz, 3H). ^{13}C NMR (176 MHz, DMSO-d_6) δ 163.1, 158.4, 158.2, 140.6, 139.8, 138.2, 134.7, 131.6, 128. 7, 127.9, 127.5, 119.7, 118.7, 108.3, 79.6, 24.2, 13.1. HRMS (ESI) m/z Calcd. $C_{21}H_{22}O_2N_5$ [M+H$^+$]: 376.1751, found 376.1768.

Cell culture and viability assay. MDA-MB-231, VERO, and A549 cell lines were maintained in Dulbecco's Modified Eagle Medium (DMEM) (Corning, 10-017-CV), supplemented with 10% fetal bovine serum (FBS) (Corning, 35-010-CV). MCF-7 cells were cultured in phenol red free Minimum Essential Medium (MEM) (Corning, 17-305-CV), supplemented with 10% fetal bovine serum (FBS). Cells were seeded into a 96-well plate (2000 cells/100uL) for 24 h prior to treatment and then treated with various drug concentrations for 72 h. All drugs were dissolved in DMSO/DMEM with DMSO concentration maintained at 1%. The effect of compounds on cell viability was measured using the MTS assay (CellTiter 96 Aqueous One Solution and CellTiter 96 Non-Radioactive Cell Proliferation Assays, Promega, Madison, WI) as described by the manufacturer. IC_{50}s were determined using Prism GraphPad 8.

***In vitro* HDAC inhibition assay.** *In vitro* HDAC inhibition assay was performed through contractual agreement with BPS Bioscience.

Western blots analysis. MDA-MB-231 cells were seeded into 6-well plate at $1*10^6$/well in DMEM for 24 h after which the cells were starved in serum-free DMEM for another 24 h. Various concentrations of SAHA, PYM and **12c** solutions in DMSO were added to the cell culture media such that the final DMSO level is 0.1%. Cells were treated for 24 h, washed with cold PBS, and lysed with RIPA buffer (110µl) (VWR, VWRVN653-100ML) buffer containing phosphatase inhibitor (Fisher Thermo, A32957) and protease inhibitor (Fisher Thermo, A32955). The cells were scraped and the lysate was collected and vortexed for 15s followed by sonication for 60s. The lysate was then centrifuged at 14000 rpm for 10 min and the supernatants were collected. The total protein concentration was determined using a BCA protein assay kit (BioVision, K813-2500). Based on the results from the BSA assay, the lysates were diluted to make equal protein concentration and 20-40µg of each lysate was loaded to each well of the TGX MIDI 4-20% gel (Biorad, cat. 5671093) and ran at 150V for 70 mins. Subsequently, the gel was transferred on to the Turbo PDVF membrane (Biorad, 1704273) and after blocking with 5% BSA for 1-2 h, the membrane was incubated overnight with Ac-Tubulin (Santa Cruz, sc-23950), Ac-H4 (Santa cruz, sc-515319), Bcl-2 (Santa Cruz, sc-7382), Bcl-xL (Santa Cruz, sc-8392), and p-STAT3/STAT3 (Cellsignal, D3A7/D1B2J) antibodies. The second day, the membrane was washed with TBST for 3x5 min. Secondary antibody (Immunoreagents, part. IR2173) was added and the membrane was incubated with agitation for 1 h. Bands were quantified using Odyssey CLx Image system.

Flow cytometry

MDA-MB-231 cells ($5*10^6$) were seeded to 10 cm plate with DMEM for 24 h prior to drug treatment. Cells were treated with DMSO (control) and DMSO solutions of SAHA (5μM) and **12b** (15μM), such that the final DMSO level is 0.1%, for another 48 h. Cells were trypsinized and washed with cold 1X PBS solution twice. Subsequently, cells were collected using 1x PBS buffer and fixed overnight at -20°C using 70% ethanol. Cells were then washed, centrifuged and re-suspended in 1X PBS; and the suspension was treated with 200ug/mL RNase for 30 min. Then cells were treated with 50ug/mL PI staining at room temperature for 30 mins. The cell cycle was analyzed with BD FACS Aria Illu Analyzer and the data was processed using FlowJo.

Acknowledgments

This work was supported by the Georgia Institute of Technology and by the Vasser-Woolley Fellowship (A.K.O.).

References

1. Cowman AF, Morry MJ, Biggs BA, Cross GA, Foote SJ. Amino acid changes linked to pyrimethamine resistance in the dihydrofolate reductase-thymidylate synthase gene of Plasmodium falciparum. *Proc Natl Acad Sci U S A*. 1988;85(23):9109-13.

2. Curd FH, Davey DG, Rose FL. Studies on synthetic antimalarial drugs; some biguanide derivatives as new types of antimalarial substances with both therapeutic and causal prophylactic activity. *Ann Trop Med Parasitol*. 1945;39:208-16.

3. James, Fraction, Deborah, Elissa, Joseph, Lisa, et al. Molecular Markers for Failure of Sulfadoxine-Pyrimethamine and Chlorproguanil-Dapsone Treatment ofPlasmodium falciparumMalaria. *The Journal of Infectious Diseases*. 2002;185(3):380-8.

4. Ferone R, Roland S. Dihydrofolate reductase: thymidylate synthase, a bifunctional polypeptide from Crithidia fasciculata. *Proc Natl Acad Sci U S A*. 1980;77(10):5802-6.

5. Kompis IM, Islam K, Then RL. DNA and RNA synthesis: antifolates. *Chem Rev*. 2005;105(2):593-620.

6. Li R, Sirawaraporn R, Chitnumsub P, Sirawaraporn W, Wooden J, Athappilly F, et al. Three-dimensional structure of M. tuberculosis dihydrofolate reductase reveals opportunities for the design of novel tuberculosis drugs. *J Mol Biol*. 2000;295(2):307-23.

7. Sharma A, Jyotsana N, Lai CK, Chaturvedi A, Görlich K, Murphy C, et al. High-throughput drug screening identifies pyrimethamine as a potent and selective inhibitor of acute myeloid leukemia. *Am Soc Hematology;* 2014.

8. Shuai K, Ziemiecki A, Wilks AF, Harpur AG, Sadowski HB, Gilman MZ, et al. Polypeptide signalling to the nucleus through tyrosine phosphorylation of Jak and Stat proteins. *Nature*. 1993;366(6455):580.

9. Weimbs T, Talbot JJ. STAT3 Signaling in Polycystic Kidney Disease. *Drug Discov Today Dis Mech*. 2013;10(3-4):e113-e8.

10. Miklossy G, Hilliard TS, Turkson J. Therapeutic modulators of STAT signalling for human diseases. *Nat Rev Drug Discov*. 2013;12(8):611-29.

11. Chaudhari S, Desai JS, Adam A, Mishra P. JAK/STAT as a novel target for treatment of leukemia. *Int J Pharm Pharm Sci*. 2014;6(1):1-7.

12. Spitzner M, Ebner R, Wolff HA, Ghadimi BM, Wienands J, Grade M. STAT3: A Novel Molecular Mediator of Resistance to Chemoradiotherapy. *Cancers (Basel)*. 2014;6(4):1986-2011.

13. Kim E, Kim M, Woo DH, Shin Y, Shin J, Chang N, et al. Phosphorylation of EZH2 activates STAT3 signaling via STAT3 methylation and promotes tumorigenicity of glioblastoma stem-like cells. *Cancer Cell*. 2013;23(6):839-52.

14. Lee H, Zhang P, Herrmann A, Yang C, Xin H, Wang Z, et al. Acetylated STAT3 is crucial for methylation of tumor-suppressor gene promoters and inhibition by resveratrol results in demethylation. *Proceedings of the National Academy of Sciences*. 2012;109(20):7765-9.

15. Alvarez JV, Febbo PG, Ramaswamy S, Loda M, Richardson A, Frank DA. Identification of a genetic signature of activated signal transducer and activator of transcription 3 in human tumors. *Cancer research*. 2005;65(12):5054-62.

16. Yeh JE, Frank DA. STAT3-Interacting Proteins as Modulators of Transcription Factor Function: Implications to Targeted Cancer Therapy. *ChemMedChem*. 2016;11(8):795-801.

17. Nelson EA, Sharma SV, Settleman J, Frank DA. A chemical biology approach to developing STAT inhibitors: molecular strategies for accelerating clinical translation. *Oncotarget*. 2011;2(6):518.

18. Chang C-H, Liu W-T, Hung H-C, Gean C-Y, Tsai H-M, Su C-L, et al. Synergistic inhibition of tumor growth by combination treatment with drugs against different subpopulations of glioblastoma cells. *BMC cancer*. 2017;17(1):905.

19. Kabra DG, Pfuhlmann K, García-Cáceres C, Schriever SC, García VC, Kebede AF, et al. Hypothalamic leptin action is mediated by histone deacetylase 5. *Nature Communications*. 2016;7:10782.

20. Gryder BE, Sodji QH, Oyelere AK. Targeted cancer therapy: giving histone deacetylase inhibitors all they need to succeed. *Future medicinal chemistry*. 2012;4(4):505-24.

21. Mottamal M, Zheng S, Huang T, Wang G. Histone deacetylase inhibitors in clinical studies as templates for new anticancer agents. *Molecules*. 2015;20(3):3898-941.

22. Tapadar S, Fathi S, Raji I, Omesiete W, Kornacki JR, Mwakwari SC, et al. A structure–activity relationship of non-peptide macrocyclic histone deacetylase inhibitors and their anti-proliferative and anti-inflammatory activities. *Bioorganic & medicinal chemistry*. 2015;23(24):7543-64.

23. Mann BS, Johnson JR, Cohen MH, Justice R, Pazdur R. FDA approval summary: vorinostat for treatment of advanced primary cutaneous T-cell lymphoma. *The oncologist*. 2007;12(10):1247-52.

24. Coiffier B, Pro B, Prince HM, Foss F, Sokol L, Greenwood M, et al. Romidepsin for the treatment of relapsed/refractory peripheral T-cell lymphoma: pivotal study update demonstrates durable responses. *Journal of hematology & oncology*. 2014;7(1):11.

25. Plumb JA, Finn PW, Williams RJ, Bandara MJ, Romero MR, Watkins CJ, et al. Pharmacodynamic response and inhibition of growth of human tumor xenografts by the novel histone deacetylase inhibitor PXD101. *Molecular cancer therapeutics*. 2003;2(8):721-8.

26. Laubach JP, Moreau P, San-Miguel JF, Richardson PG. Panobinostat for the treatment of multiple myeloma. *Clinical cancer research*. 2015;21(21):4767-73.

27. Ning Z-Q, Li Z-B, Newman MJ, Shan S, Wang X-H, Pan D-S, et al. Chidamide (CS055/HBI-8000): a new histone deacetylase inhibitor of the benzamide class with antitumor activity and the ability to enhance immune cell-mediated tumor cell cytotoxicity. *Cancer chemotherapy and pharmacology*. 2012;69(4):901-9.

28. Gupta K, Gulen F, Sun L, Aguilera R, Chakrabarti A, Kiselar J, et al. GSK3 is a regulator of RAR-mediated differentiation. *Leukemia*. 2012;26(6):1277.

29. Zeng H, Qu J, Jin N, Xu J, Lin C, Chen Y, et al. Feedback Activation of Leukemia Inhibitory Factor Receptor Limits Response to Histone Deacetylase Inhibitors in Breast Cancer. *Cancer Cell*. 2016;30(3):459-73.

30. Mwakwari SC, Guerrant W, Patil V, Khan SI, Tekwani BL, Gurard-Levin ZA, et al. Non-peptide macrocyclic histone deacetylase inhibitors derived from tricyclic ketolide skeleton. *Journal of medicinal chemistry*. 2010;53(16):6100-11.

31. Tropak MB, Zhang J, Yonekawa S, Rigat BA, Aulakh VS, Smith MR, et al. Pyrimethamine derivatives: insight into binding mechanism and improved enhancement of mutant β-N-acetylhexosaminidase activity. *Journal of medicinal chemistry*. 2015;58(11):4483-93.

32. Love MI, Huber W, Anders S. Moderated estimation of fold change and dispersion for RNA-seq data with DESeq2. *Genome biology*. 2014;15(12):550.

33. Liu H, Qin Y, Zhai D, Zhang Q, Gu J, Tang Y, et al. Antimalarial Drug Pyrimethamine Plays a Dual Role in Antitumor Proliferation and Metastasis through Targeting DHFR and TP. *Molecular cancer therapeutics*. 2019;18(3):541-55.

34. Ji Y, Trenkle WC, Vowles JV. A high-yielding preparation of β-ketonitriles. *Organic letters*. 2006;8(6):1161-3.

35. Kuroyanagi J-i, Kanai K, Sugimoto Y, Fujisawa T, Morita C, Suzuki T, et al. Novel antifungal agents: Triazolopyridines as inhibitors of β-1, 6-glucan synthesis. *Bioorganic & medicinal chemistry*. 2010;18(16):5845-54.

36. Chan DC, Fu H, Forsch RA, Queener SF, Rosowsky A. Design, synthesis, and antifolate activity of new analogues of piritrexim and other diaminopyrimidine dihydrofolate reductase inhibitors with ω-carboxyalkoxy or ω-carboxy-1-alkynyl substitution in the side chain. *Journal of medicinal chemistry*. 2005;48(13):4420-31.

37. Porcheddu A, Giacomelli G, Piredda I, Carta M, Nieddu G. A practical and efficient approach to PNA monomers compatible with Fmoc-mediated solid-phase synthesis protocols. *European Journal of Organic Chemistry*. 2008;2008(34):5786-97.

38. Dhokale B, Jadhav T, Mobin SM, Misra R. Meso alkynylated tetraphenylethylene (TPE) and 2, 3, 3-triphenylacrylonitrile (TPAN) substituted BODIPYs. *The Journal of organic chemistry*. 2015;80(16):8018-25.

39. Rostovtsev VV, Green LG, Fokin VV, Sharpless KB. A stepwise huisgen cycloaddition process: copper (I)-catalyzed regioselective "ligation" of azides and terminal alkynes. *Angewandte Chemie International Edition*. 2002;41(14):2596-9.

40. Gryder BE, Akbashev MJ, Rood MK, Raftery ED, Meyers WM, Dillard P, et al. Selectively targeting prostate cancer with antiandrogen equipped histone deacetylase inhibitors. *ACS chemical biology*. 2013;8(11):2550-60.

41. De Savi C, Bradbury RH, Rabow AA, Norman RA, de Almeida C, Andrews DM, et al. Optimization of a Novel Binding Motif to (E)-3-(3, 5-Difluoro-4-((1 R, 3 R)-2-(2-fluoro-2-methylpropyl)-3-methyl-2, 3, 4, 9-tetrahydro-1 H-pyrido [3, 4-b] indol-1-yl) phenyl) acrylic Acid (AZD9496), a Potent and Orally Bioavailable Selective Estrogen Receptor Downregulator and Antagonist. *Journal of medicinal chemistry*. 2015;58(20):8128-40.

42. Liu W, Lau F, Liu K, Wood HB, Zhou G, Chen Y, et al. Benzimidazolones: A new class of selective peroxisome proliferator-activated receptor γ (PPARγ) modulators. *Journal of medicinal chemistry*. 2011;54(24):8541-54.

43. Garber SB, Kingsbury JS, Gray BL, Hoveyda AH. Efficient and recyclable monomeric and dendritic Ru-based metathesis catalysts. *Journal of the American Chemical Society*. 2000;122(34):8168-79.

44. Bramati A, Girelli S, Torri V, Farina G, Galfrascoli E, Piva S, et al. Efficacy of biological agents in metastatic triple-negative breast cancer. *Cancer Treat Rev*. 2014;40(5):605-13.

45. Podo F, Santoro F, Di Leo G, Manoukian S, de Giacomi C, Corcione S, et al. Triple-Negative versus Non-Triple-Negative Breast Cancers in High-Risk Women: Phenotype Features and Survival from the HIBCRIT-1 MRI-Including Screening Study. *Clin Cancer Res*. 2016;22(4):895-904.

46. Aryappalli P, Al-Qubaisi SS, Attoub S, George JA, Arafat K, Ramadi KB, et al. The IL-6/STAT3 Signaling Pathway Is an Early Target of Manuka Honey-Induced Suppression of Human Breast Cancer Cells. *Front Oncol*. 2017;7:167.

47. Banerjee K, Resat H. Constitutive activation of STAT3 in breast cancer cells: A review. *Int J Cancer*. 2016;138(11):2570-8.

48. Schütz A, Röser K, Klitzsch J, Lieder F, Aberger F, Gruber W, et al. Lung adenocarcinomas and lung cancer cell lines show association of MMP-1 expression with STAT3 activation. *Translational oncology*. 2015;8(2):97-105.

49. Yu X, He L, Cao P, Yu Q. Eriocalyxin B inhibits STAT3 signaling by covalently targeting STAT3 and blocking phosphorylation and activation of STAT3. *PLoS One*. 2015;10(5):e0128406.

50. Berishaj M, Gao SP, Ahmed S, Leslie K, Al-Ahmadie H, Gerald WL, et al. Stat3 is tyrosine-phosphorylated through the interleukin-6/glycoprotein 130/Janus kinase pathway in breast cancer. *Breast Cancer Research*. 2007;9(3):R32.

51. Aldinucci D, Colombatti A. The inflammatory chemokine CCL5 and cancer progression. *Mediators of inflammation*. 2014;2014.

52. Li L, Shaw PE. Autocrine-mediated activation of STAT3 correlates with cell proliferation in breast carcinoma lines. *Journal of Biological Chemistry*. 2002;277(20):17397-405.

53. Garcia R, Bowman TL, Niu G, Yu H, Minton S, Muro-Cacho CA, et al. Constitutive activation of Stat3 by the Src and JAK tyrosine kinases participates in growth regulation of human breast carcinoma cells. *Oncogene*. 2001;20(20):2499.

54. Sodji QH, Kornacki JR, McDonald JF, Mrksich M, Oyelere AK. Design and structure activity relationship of tumor-homing histone deacetylase inhibitors conjugated to folic and pteroic acids. *European journal of medicinal chemistry*. 2015;96:340-59.

55. Bantscheff M, Hopf C, Savitski MM, Dittmann A, Grandi P, Michon A-M, et al. Chemoproteomics profiling of HDAC inhibitors reveals selective targeting of HDAC complexes. *Nature biotechnology*. 2011;29(3):255.

56. Epling-Burnette PK, Liu JH, Catlett-Falcone R, Turkson J, Oshiro M, Kothapalli R, et al. Inhibition of STAT3 signaling leads to apoptosis of leukemic large granular lymphocytes and decreased Mcl-1 expression. *Journal of Clinical Investigation*. 2001;107(3):351-62.

57. Xiong A, Yang Z, Shen Y, Zhou J, Shen Q. Transcription Factor STAT3 as a Novel Molecular Target for Cancer Prevention. 2014;6(2):926-57.

58. Hata AN, Engelman JA, Faber AC. The BCL2 family: key mediators of the apoptotic response to targeted anticancer therapeutics. *Cancer discovery*. 2015;5(5):475-87.

59. Lin L, Hutzen B, Zuo M, Ball S, Deangelis S, Foust E, et al. Novel STAT3 phosphorylation inhibitors exhibit potent growth-suppressive activity in pancreatic and breast cancer cells. *Cancer research*. 2010;70(6):2445-54.

60. Cheng X, Peuckert C, Wolfl S. Essential role of mitochondrial Stat3 in p38(MAPK) mediated apoptosis under oxidative stress. *Sci Rep*. 2017;7(1):15388.

61. Liu J, Qu X, Shao L, Hu Y, Yu X, Lan P, et al. Pim-3 enhances melanoma cell migration and invasion by promoting STAT3 phosphorylation. *Cancer Biol Ther*. 2018;19(3):160-8.

62. Yeh JE. Molecular Modulators of the Oncogenic Transcription Factor STAT3. Doctoral dissertation, Harvard University, Graduate School of Arts & Sciences.2015.

63. Huang L, Pardee AB. Suberoylanilide hydroxamic acid as a potential therapeutic agent for human breast cancer treatment. *Mol Med*. 2000;6(10):849-66.

Pyrimethamine Conjugated Histone Deacetylase inhibitors: Design, Synthesis and Evidence for Triple Negative Breast Cancer Selective Cytotoxicity.

Bocheng Wu[1†], Shaghayegh Fathi[1, 2†], Shanee Mortley[1], Mahir Mohiuddin[4, 5], Young C. Jang[3, 4, 5], Adegboyega Oyelere[1, 4*]

School of Chemistry and Biochemistry, School of Biological Sciences, Parker H. Petit Institute for Bioengineering and Bioscience, Georgia Institute of Technology, Atlanta, GA 30332-0400 USA

[1]School of Chemistry and Biochemistry, Georgia Institute of Technology

[2]Current Address: University of Chicago

[3]School of Biological Sciences, Georgia Institute of Technology

[4]Parker H. Petit Institute for Bioengineering and Bioscience, Georgia Institute of Technology

[5]Wallace H. Coulter Department of Biomedical Engineering, Georgia Institute of Technology

[†]These Authors contributed equally to the manuscript

Correspondence to:

Adegboyega K. Oyelere, **E-mail:** aoyelere@gatech.edu

Keywords: Pyrimethamine, STAT proteins, STAT3, histone deacetylases, histone deacetylase inhibitors, Triple Negative Breast Cancer, molecular docking

Graphical Abstract

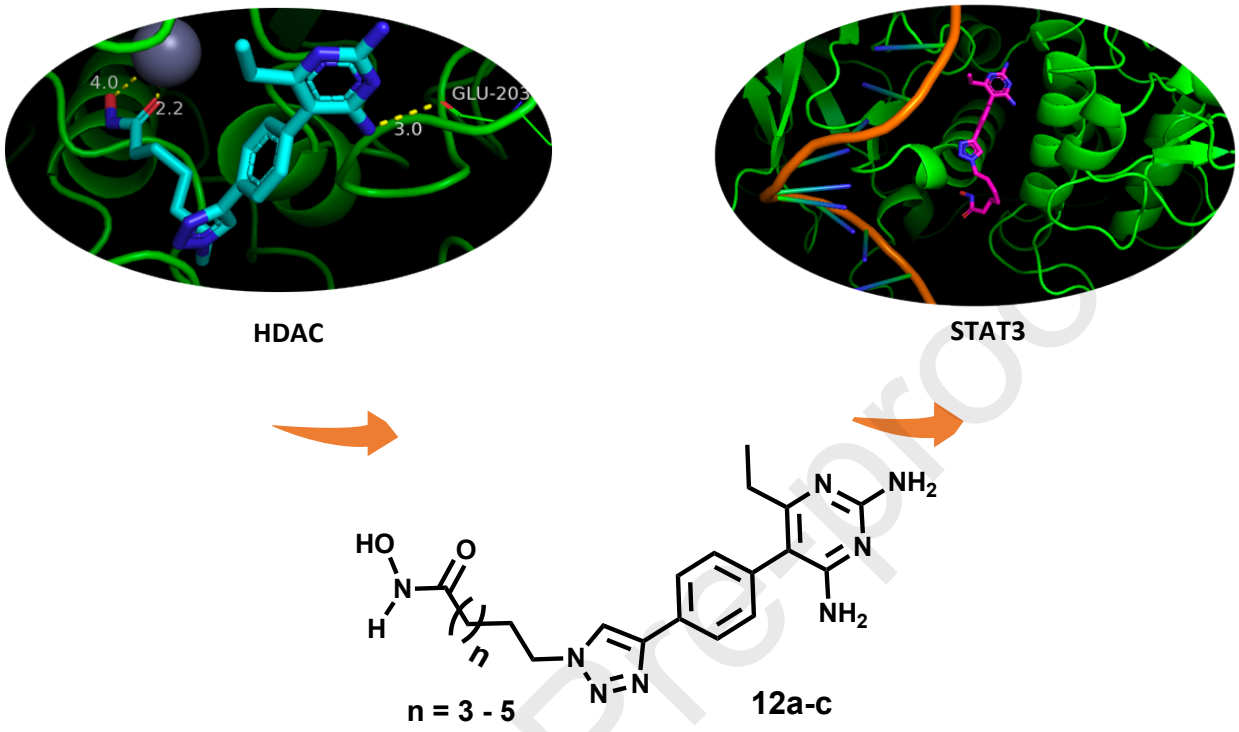

Pyrimethamine Conjugated Histone Deacetylase inhibitors: Design, Synthesis and Evidence for Triple Negative Breast Cancer Selective Cytotoxicity.

Bocheng Wu[1†], Shaghayegh Fathi[1, 2†], Shanee Mortley[1], Mahir Mohiuddin[4, 5], Young C. Jang[3, 4, 5], Adegboyega Oyelere[1, 4*]

School of Chemistry and Biochemistry, School of Biological Sciences, Parker H. Petit Institute for Bioengineering and Bioscience, Georgia Institute of Technology, Atlanta, GA 30332-0400 USA

[1]School of Chemistry and Biochemistry, Georgia Institute of Technology

[2]Current Address: University of Chicago

[3]School of Biological Sciences, Georgia Institute of Technology

[4]Parker H. Petit Institute for Bioengineering and Bioscience, Georgia Institute of Technology

[5]Wallace H. Coulter Department of Biomedical Engineering, Georgia Institute of Technology

[†]These Authors contributed equally to the manuscript

Correspondence to:

Adegboyega K. Oyelere, **E-mail:** aoyelere@gatech.edu

Keywords: Pyrimethamine, STAT proteins, STAT3, histone deacetylases, histone deacetylase inhibitors, Triple Negative Breast Cancer, molecular docking

Conflict of Interest Statement: The Authors have no conflict.